

# A Scalable Platform for Distributed Object Tracking across a Many-camera Network

Aakash Khochare\*, Aravindhnan Krishnan and Yogesh Simmhan\*

*\*Department of Computational and Data Sciences  
Indian Institute of Science, Bangalore, India*

*EMail: aakhochare@IISc.ac.in, simmhan@IISc.ac.in*

## Abstract

Advances in deep neural networks (DNN) and computer vision (CV) algorithms have made it feasible to extract meaningful insights from large-scale deployments of urban cameras. Tracking an object of interest across the camera network in near real-time is a canonical problem. However, current tracking platforms have two key limitations: 1) They are monolithic, proprietary and lack the ability to rapidly incorporate sophisticated tracking models; and 2) They are less responsive to dynamism across wide-area computing resources that include edge, fog and cloud abstractions. We address these gaps using *Anveshak*, a runtime platform for composing and coordinating distributed tracking applications. It provides a domain-specific dataflow programming model to intuitively compose a tracking application, supporting contemporary CV advances like query fusion and re-identification, and enabling dynamic scoping of the camera network’s search space to avoid wasted computation. We also offer tunable batching and data-dropping strategies for dataflow blocks deployed on distributed resources to respond to network and compute variability. These balance the tracking accuracy, its real-time performance and the active camera-set size. We illustrate the concise expressiveness of the programming model for 4 tracking applications. Our detailed experiments for a network of 1000 camera-feeds on modest resources exhibit the tunable scalability, performance and quality trade-offs enabled by our dynamic tracking, batching and dropping strategies.

# 1 Introduction

The push for smarter and safer cities has led to the proliferation of video cameras in public spaces. Regions like London, New York, Singapore and China [1, 12] have deployed camera networks with 1000’s of feeds to help with *urban safety*, e.g., to detect abandoned objects [46], to track missing people [13] and for behavioral analysis [33]. They are also used for *citizen services*, e.g., to identify open parking spots and count the traffic flow [43]. Such “many-camera networks”, when coupled with sophisticated Computer Vision (CV) algorithms and Deep Learning (DL) models [35], can also serve as *meta-sensors* to replace other physical sensors for IoT applications and to complement on-board cameras for self-driving cars [32].

One canonical application domain that operates over such ubiquitous video feeds is called *tracking* [14]. Here, the goal is to *identify an “object”* or “entity” (e.g., a stolen vehicle or a missing child), based on a given sample image or feature vector, in video streams arriving from cameras distributed across the city, and to *track that entity’s movements* across the many-camera network in near real-time [44]. Fig. 1 illustrates a *missing person* being tracked across a network of 5 video cameras,  $C_A-C_E$ , on a road network using a smart *spotlight* tracking algorithm. A blue circle indicates the *Field of View (FOV)* of a camera. The path taken by the person between time  $t_1$  and  $t_5$  is indicated by the blue dashed arrow. Given an image of the person, the goal is to locate and trace the path taken by them across the region with high accuracy, while reducing the application design and computing overheads. These poses several challenges.

**Challenge 1 (Composability).** The application requires online video analytics across space and time, and this commonly has three stages: *object detection*, *object tracking*, and *re-identification* [14]. The first filters out objects that do not belong to the same class as the entity while the second follows the motion of objects in a single camera’s frame [54]. Re-identification (or re-id) matches the objects in a camera with the given target entity [39]. Recently, a fourth stage called *fusion* enhances the original entity query with features from the matched images that is then used for tracking, giving better accuracy [42].

Each of these individual problems is well-researched. But these stages have to be *composed* as part of an overall platform, and coupled with a *distributed tracking logic* that operates across the camera network and over time. However, contemporary many-camera analysis platforms are *monolithic, proprietary, and bespoke* [37, 52]. They offer limited composability and reusability of models, and minimal support for custom tracking strategies. This increases the *time and effort* to incorporate domain intelligence and adopt the rapid advances being made in CV/DL.

**Challenge 2 (Distributed Tracking).** It is impractical to execute the full video analytics pipeline on all the cameras due to the punitive computing and network costs. E.g., just doing object detection on a 1000-camera network using a contemporary fast neural network requires 5–128 Titan XP GPUs, depending on the video resolution and frame-rate, besides the bandwidth to move the video streams to the compute resource [47]. Instead, these platforms should

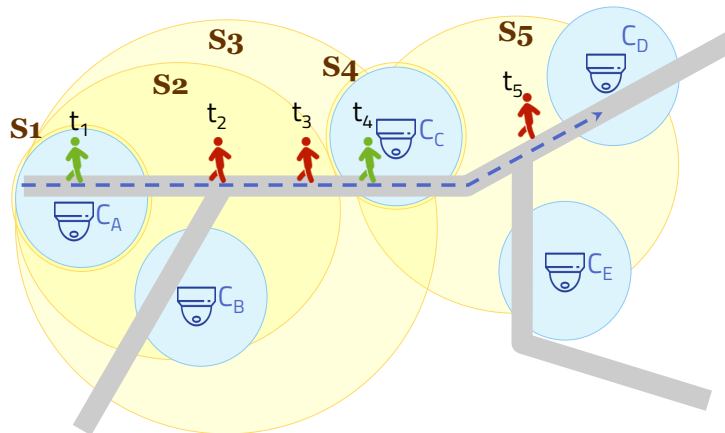


Figure 1: *Spotlight* strategy for camera activation while tracking. Blue circles are the FOV of cameras  $C_A$ – $C_E$ . The person icon shows the location of the person at times  $t_1$ – $t_5$  on the road; a red icon means they are in a blind-spot while a green icon means they are in the FOV of a camera. The yellow circles  $S_i$  are the calculated spotlight regions that indicate the cameras that should be active at time  $t_i$ .

incorporate *smart tracking strategies* that limit the video processing to the cameras where the object is likely to be present and adapt to *blind-spots* [24]. They can use domain knowledge like the road and transit network, speed of the object, camera location and field of view to make smart choices on the video streams to be actively processed.

**Example.** In Fig. 1, the cameras need not generate and process video feeds unless *activated*. Initially, at time  $t_1$ , the person is within the FOV of  $C_A$ , and only this camera is made active. By time  $t_2$ , they have moved out of the FOV of  $C_A$ , and also of all other cameras, i.e., in a *blind-spot*. Now, we calculate a *spotlight* neighborhood around the camera in which they were last seen, and *activate* cameras that fall within this region, as shown by the yellow circle  $S_2$ , which overlaps with  $C_A$  and  $C_B$ . This spotlight grows in size to  $S_3$  at time  $t_3$  as the person is still in a blind-spot, and it activates camera  $C_C$  as well. The person reappears in the FOV of  $C_C$  at time  $t_4$  and the spotlight shrinks to  $S_4$  with just this single camera being active and the rest are *deactivated*. The spotlight again grows at time  $t_5$  when the person is lost, and  $S_5$  activates cameras  $C_C$ ,  $C_D$  and  $C_E$ . ■

Using such a smart tracking logic to scope the region of interest can significantly reduce the number of active video streams we process, e.g., to 1–3 cameras rather than all 5, in Fig. 1. This reduces the resource usage substantially with limited impact on the tracking accuracy. However, contemporary many-camera analysis platforms do not offer such sophisticated and customizable tracking logic.

**Challenge 3 (Edge computing and Scaling).** Smart cities are seeing *edge and fog computing resources* being deployed on Metropolitan Area Networks (MAN), to complement *cloud resources* [56]. This brings processing closer to the data source and conserves network bandwidth [15, 41]. This is important for video tracking, given its low latency, high bandwidth and high compute needs [12, 48]. So tracking platforms must effectively use such heterogeneous, wide-area compute resources that are part of the computing continuum rather than rely exclusively on cloud resources.

For *scalability*, the platform must balance the latency for tracking against the throughput supported for the active camera feeds on the available resources – a high latency can cause the object to be detected late, and lead to the spotlight region growing larger when the person is missing, while a low throughput can limit the number of cameras that can be active at a time, and increase the chances of losing the person. Also, given the *dynamism* in the network behavior, compute performance and stream rates, the platform must trade-off the accuracy of tracking with the application’s performance at runtime. *Current platforms do not offer such tunable adaptivity and scaling* [25, 44].

We make the following specific contributions in this article to address these challenges:

1. We propose a novel *domain-specific dataflow model* for current and emerging tracking applications, with functional operators to plug-in different analytics. Uniquely, it has first-class support for *distributed tracking strategies* to dynamically decide the active cameras (§ 2). These address Challenges 1 and 2.
2. We implement the dataflow model and heuristics in our *Anveshak platform* to execute across distributed edge, fog and cloud resources (§ 3). Further, it incorporates domain-sensitive heuristics for *dropping and batching frames*, which allow users to tune the accuracy, the latency and the scalability under dynamism (§ 4). These address Challenge 3.
3. We illustrate the *flexibility* of the dataflow model using 4 tracking applications, and offer detailed empirical results across latency, accuracy, camera-set sizes and tracking logic to validate the *scalability and tunability* of our platform (§ 5).

We complement these with a review of related work in § 6 and offer our conclusions in § 7.

## 2 A Dataflow Model for Tracking

We first discuss the features of a generic many-camera infrastructure, and then propose a domain-specific dataflow programming model to compose tracking applications.

## 2.1 System Model

A many-camera infrastructure consists of a set of cameras that are statically placed at specific locations in a city, and each can generate a stream of video observations within its FOV [44]. The cameras are connected to a MAN, directly or through an edge computing device [48]. (Accelerated) Fog devices may be co-located with the cameras or within a few network hops of them, while cloud resources are accessible at data centers over the Wide Area Network (WAN) [56]. While the edge and fog are typically captive city resources, cloud resources are available on-demand for a price. These resource classes have heterogeneous capacities, and their performance may *vary over time* due to multi-tenancy. The bandwidth and latency between devices on the MAN and the WAN can be *dynamic*, depending on the traffic. These can affect the QoS of distributed applications.

Cameras allow remote access to their video streams over the network and expose endpoints to control parameters such as the frame rate, resolution and FOV [29]. Traditionally, servers in the city’s control center or in the cloud would acquire the streams for visualization, real-time analytics and archival. But, moving all video data to the compute incurs high bandwidth, and analyzing all streams in real-time can be compute-intensive. Instead, we propose to move the analytics to the data by using edge and fog devices close to the cameras, complemented by the cloud for control. Hence, the tracking platform must operate on heterogeneous, dynamic and distributed compute and network resources.

## 2.2 Domain-specific Programming Model

We propose a domain-specific model for tracking applications as a *streaming dataflow* with pre-defined *modules* (Fig. 2). The user provides the functional *logic* for these modules to compose an application by consuming and producing streams of events (e.g., video frames, detections). We specify the input and output *interfaces* for each module. Multiple *instances* of a module can naturally execute different input events in a data-parallel manner.

The modules are analogous to the APIs offered by Apache Spark and Hadoop MapReduce [22, 57] for pre-defined tasks. However, rather than a general-purpose dataflow like Spark [57], our domain-specific dataflow composition is fixed. This is like MapReduce [22] where the user specifies the *Map* and *Reduce* logic, but the dataflow and execution pattern is pre-defined. This eases the development of tracking applications. Users can focus on contemporary and emerging advances in DL/CV models that are incorporate into the analytics modules, and uniquely, control the distributed tracking logic through a custom module. Further, our runtime platform offers the benefits of automatic parallelization and performance management.

Next we describe the interfaces of these modules, the dataflow pattern, and the execution model (Fig. 2).

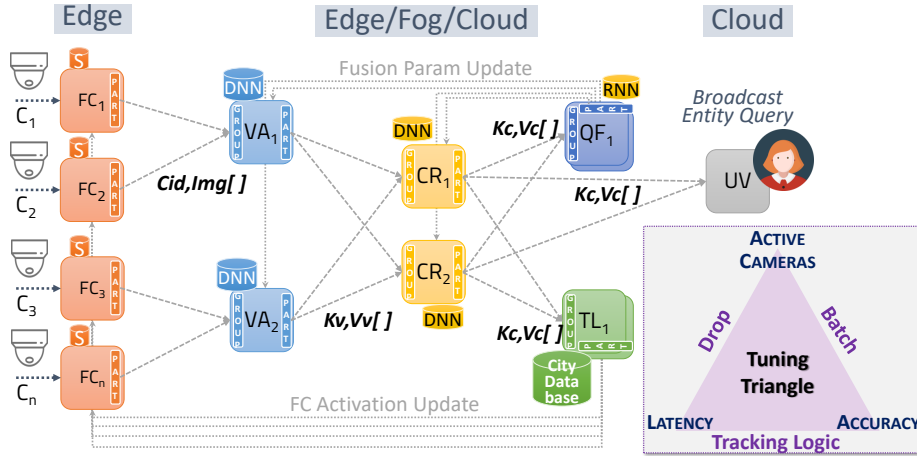


Figure 2: Domain-specific dataflow and modules for tracking. (Inset) Tunable performance and scalability choices.

### 2.2.1 Filter Controls (FC)

This module is the entry point for video frames from a camera into the dataflow. It is usually co-located with the camera or on an *edge device* connected to it. Each camera has a single FC instance along with its *local state*. Its user-logic decides if a video frame on the input stream of an FC should be forwarded on its output stream to the Video Analytics (VA) module, or ignored. FC uses its local state (e.g., *isActive*) or even the frame content to decide this. If a frame is forwarded, a key-value event is sent on the output stream, with camera ID as key and frame content as value.

Importantly, the FC state for a camera can be *updated* by control events from the Tracking Logic (TL), as described in § 2.2.4. This allows *tunable activation* of video streams that will enter the dataflow, on a per-camera basis. E.g., TL can have FC deactivate a camera feed if the target will not be present in its FOV, or reduce/increase the frame-rate based on the target’s speed. This can balance the dataflow’s performance and accuracy. The FC logic should be simple as it runs on edge devices.

### 2.2.2 Video Analytics (VA)

This module receives input event streams from one or more upstream FC modules, and performs *video analytics on a single camera’s stream* at a time. This has access to the *entity query* provided by the user, e.g., an image of a person. The user-logic for this module can be complex, and invoke external models in *TensorFlow*, *PyTorch* or *OpenCV*. The input API for the logic is an iterator of events, *grouped* by the camera ID. This is similar to the *shuffle and reduce* in MapReduce. Grouping by camera ID gives the logic access to a *batch of frames* from the same camera for temporal analytics. This also amortizes the overheads

to invoke the external models. We discuss specific batching strategies in § 4.4. Depending on the compute needs of this logic, it may run on edge, fog or cloud resources.

Exemplar VA logic include object detection and tracking using DL models like *YOLOv2* [47] or classic CV techniques like *Histogram of Gradients (HoG)*. VA can access the user’s target query and maintain *local state* across executions, to be passed to the external model. The output of the logic is a batch of key-value pairs, which may be, e.g., the camera ID (key), and bounding boxes for potential target objects in a frame with confidence scores (value). There can be a many-to-many relationship between the input and output events for this module. However, we allow users to *link* an output event with an input event, and this provenance lets us trace its latency and help with drop strategies we propose in § 4.3 to meet the QoS goals.

Like FC, the local state of this module can be updated by the *Query Fusion (QF)* task. This allows dynamic updates to the entity query by *fusion* algorithms [42] to enhance a query’s feature vector with information from ongoing detections of the entity in the frames. The VA can also update its model based on such signals.

### 2.2.3 Contention Resolution (CR)

This module receives a stream of key-value events from one or more VA instances, *grouped by key*. The keys are typically the camera ID and the values contain detections or annotated frames, but these can be overridden by the VA user logic. It has access to the entity query as well. This logic is used to analyze results from *multiple cameras*, say, to resolve conflicting detections from different cameras, e.g., the same entity being detected at different parts of the city simultaneously. It can use more advanced re-id logic or DL models for a *higher accuracy match*. CR may be triggered only on a conflict or a low confidence detection by a VA, and hence execute less often than VA, but be compute intensive. CR may even degenerate to a human-in-the-loop deciding on borderline detections. This makes it better suited for running on fog or cloud resources. Like VA, this module can receive updates from QF as well.

The output stream from executing CR primarily contains metadata – much smaller than the video input – and this is forked three ways, to TL, QF and UV modules.

### 2.2.4 Tracking Logic (TL)

This is a *novel module* that we propose to help users capture the core logic of distributed tracking across the multi-camera network [50]. The detections that TL receives from CR for each frame may be *positive* or *negative*. On a negative detection, the TL logic is expected to *expand* the search space by activating additional cameras, while if the entity is found in a frame (positive), TL should *contract* the search space. The module also use sophisticated tracking algorithms using prior domain knowledge on the environment and the entity,

and devise strategies to (de)activate the cameras to optimize the quality and performance of tracking. It can be hosted on cloud resources.

E.g., in Fig. 1, TL can use the knowledge of the road network and camera locations to dynamically decide the camera search space (spotlight), depending on when and in which camera the entity was last detected, and (de)activate those cameras. It can also be more sophisticated and change the FOV for cameras to focus on an approaching or receding entity, or change the frame-rate based on the entity’s speed. This separates the core video analytics logic, from their interpretation over the camera network for distributed entity tracking and camera controls.

### 2.2.5 Query Fusion (QF)

This module uses information on the detections to enhance the entity query’s features. High-confidence entity detections in the input video can be fused with the existing entity query to generate a new query that offers better matches, or even use negative matches to enhance the query [42, 50]. The output of this module updates the entity query at the VA and CR modules for their future input streams.

### 2.2.6 User Visualization (UV)

This is a user-facing module that can be used to submit the entity query and display the current state of the tracking and detections. This can be a central portal running on the cloud where authorized personnel can view the progress.

### 2.2.7 Discussion on Event Ordering

The programming model and runtime do not enforce *temporal ordering* of events flowing across different streams in the pipeline. While *temporal ordering* may be required for some vision algorithms such as estimating optical flow [26], the user logic can reorder events in a batch using the timestamps passed in the *key, value* pairs. The runtime can enforce ordering in the *group* stage of every module using a temporal window and watermarks [10]. However, we currently do not include such mechanisms.

## 2.3 Sample Tracking Applications

We illustrate several applications designed using our domain-specific dataflow and modules to track an *entity* (e.g., missing person) across a road network. They take an input image as the entity query, and return detections of the entity in the camera network to the UV module in real-time. For the first variant (*App 1*), the pseudo-code of the user-logic for different modules are given below.

Initially, all FCs have their *active* state set to *true* to allow their input streams to be passed on, and the entity to be found for the first time. The VA gets a batch of images from a camera, and uses a feature-based OpenCV HoG

---

**Algorithm 1** Pseudocode of Modules for App 1

---

```
1: procedure FC(img, state)
2:   return state.get('isActive')
3: end procedure


---


1: procedure VA(Cid, imgs[ ], state)
2:   bbs[ ][ ] = OPENCV.HOG(imgs[ ])
3:   for img in imgs[ ] and outbbs[ ] in bbs[ ][ ] do
4:     EMIT(Cid, (img, outbbs[ ]))
5:   end for
6: end procedure


---


1: procedure CR(Cid, (img, outbbs[ ])[ ], state)
2:   query = state.get('entity_query_img')
3:   cropped = [ ]
4:   for tuple in (img, outbbs[ ])[ ] do
5:     cropped_img = CROP(img, outbbs[ ])
6:     cropped.append(cropped_img)
7:   end for
8:   detections = TFLOW.DNN_CR(cropped, query)
9:   for was_detected in detections[ ] do
10:    EMIT(Cid, (img, was_detected))
11:  end for
12: end procedure


---


1: procedure TL_WBFS((Cid, (img, detections[ ])[ ])[ ], state )
2:   el = GETENTITYLOCATION((Cid, detections[ ])[ ])
3:   if el == ∅ then           ▶ Entity lost. Expand spotlight...
4:     graph = state.get('road_network')
5:     lsl = state.get('lastSeenLocation')
6:     lst = state.get('lastSeenTime')
7:     cameras[ ] = WEIGHTEDBFS(graph, lsl, lst)
8:     EXPANDSEARCHSPACE(cameras)
9:   else
10:    SHRINKSEARCHSPACE(el)
11:  end if
12: end procedure


---


1: procedure QF((Cid, (img, detections[ ])[ ])[ ], state)
2:   oldFeature ← state.get('state')
3:   for image in img[ ] do
4:     if detection == true then
5:       newFeature ← RNN(image, oldFeature)
6:     end if
7:   end for
8:   emit(Call, image[ ], out[ ])
9: end procedure


---


```

pedestrian detector [20] to put bounding boxes (*bbs*) around persons in each

Table 1: Module mappings for illustrative tracking apps

App#	FC	VA	CR	TL	QF
1	Ac-tive?	HoG [20]	Person Re-id [2]	WBFS	–
2	Ac-tive?	HoG [20]	Person Re-id [8]	BFS	RNN [42]
3	Frame Rate	YOLO for Cars [47]	Car Re-id [53]	WBFS w/ speed	–
4	Ac-tive?	Person Re-id (Small) [28]	Person Re-id (Large) [54]	Probabilistic	–

image, and sends these to CR. HoG runs on the entire batch of images.

CR crops and extracts the image regions in the bounding boxes of frames sent from different cameras, and passes these as a batch to a high-quality OpenReid TensorFlow DNN for pedestrian detection [2]. The DNN detects if the query entity is present in the cropped images, and emits the *true* and *false* matches downstream. UV then displays the matching camera frames.

TL also receives these detections, and has access to the road network, road lengths and camera locations. When the entity is not in matched in any camera, it starts a *Weighted Breadth First Search (WBFS)* on the road network from the last known position of the entity, taking into account the road lengths, the entity’s default speed and the time elapsed since the last detection. This identifies the spotlight region where the entity should be present within, and TL contacts the FC of cameras in this region to activate them. Else, if the entity is detected in some camera’s frame, the spotlight region contracts to that camera. Lastly, QF uses an RNN [42] to enhance the entity query using high-quality hits.

Table 1 lists the module logic used in this and 3 other tracking applications we can compose. We use a different DNN [8] in CR for *App 2*. The query may also be for a vehicle based on image rather than license plate, in *App 3*, where we also use DNNs for object detection in VA [47] and CR [53]. Here, TL can also be more complex, with awareness of the road lengths and the target’s speed. In *App 4*, we can use a Naïve Bayes model to give the likelihood of paths that will be taken by the entity to decide the cameras to activate.

### 3 Anveshak Platform Implementation

We implement this domain-specific dataflow model as *Anveshak (Explorer)*, in Sanskrit), a Python-based distributed runtime engine that allows users to easily define their tracking application. Its architecture is illustrated in Fig. 3. Anveshak is more *light-weight* than Big Data streaming platforms like Apache Spark Streaming or Flink [19, 57], and designed to operate on a WAN than a Local Area Network (LAN). This allows it to be deployed on *edge, fog or cloud* resources.

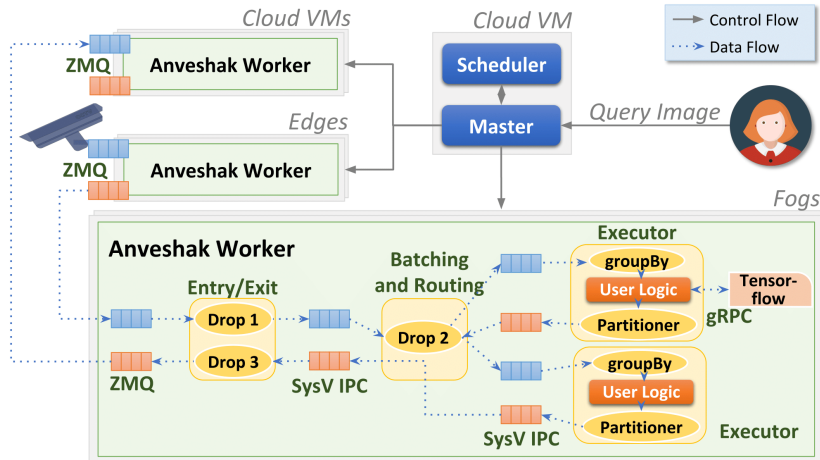


Figure 3: System Architecture of Anveshak

Application developers implement their user logic in Python for the different modules of the dataflow, such as in Table 1. External models like TensorFlow are invoked from a module using a local *gRPC* service. A *Master* process runs in the cloud at a well-known endpoint and manages the application deployment. The application definition is submitted to the Master with the module descriptions and their configuration parameters, e.g., the entity query image for VA and CR, or the expected entity speed used by TL.

The Master calls a *Scheduler* logic that decides the number of module instances and maps them to the resources. The scheduling logic is modular. By default, we use a simple round-robin scheduler with a fixed number of instances per module type, and map specific module types to specific edge, fog or cloud resource abstractions. More advanced scheduling strategies are beyond the scope of this paper.

Each distributed resource available for deploying the dataflow runs a *Worker* process, which manages module instances on that resource and transfers data between instances on different devices using *ZeroMQ* [9]. The Master initializes module instances on a resource by contacting its Worker. We assume that the required libraries are pre-deployed in the Workers, and in future, this can be replaced by light-weight containers like *minikube* [4] for deployment.

A Worker can host multiple module instances that has the user logic, and each is encapsulated in a separate *Executor* process. We use a *Router* logic to pass data between the Worker and the local Executors using *Sys V* for Inter-Process Communication (IPC) [16]. A Worker can fetch the camera feeds from an external endpoint to initiate the dataflow.

Next, we discuss various dynamic runtime optimization strategies incorporated in the Anveshak platform to balance the latency performance, detection accuracy and scalability for a tracking dataflow that is executing.

## 4 Runtime Tuning Strategies

The Anveshak platform operates in a dynamic environment, and needs to be tuned at runtime to adapt to these conditions. We offer a novel *Tuning Triangle* (Fig. 2, bottom right), where users can achieve two of three *properties*: *performance*, *accuracy* and *scalability* (shown at the corners of the triangle) when performing tracking, and these are controlled by *knobs* (shown at the side opposite to a property’s corner). The *batching* knob controls the latency property, the *dropping* knob controls the accuracy, and the sophistication of the *tracking logic* knob, already discussed, determines the active camera set size (or scalability). Next, we discuss the two other knobs to control *data drops* and *batching*.

### 4.1 Approach

We have a captive set of edge, fog and cloud resources having variable compute load due to a changing active set size being processed, and are connected over a MAN/WAN that exhibits dynamism in the latency and bandwidth between resources present on it. So the transient load on resources hosting the active module instances can exceed the available compute or network capacity, which leads to higher event latencies that can cascade up the input event stream.

In such cases, we can gracefully degrade by *dropping events* that cannot be processed within a *maximum tolerable latency* ( $\gamma$ ) specified by the user. If we drop potentially stale events early in the dataflow pipeline, we can make more resources available to the events that are retained and increase their chances of completing within the threshold. This knob helps meet the latency goals and supports a larger active-set size, but it affects the accuracy of tracking if frames containing the entity are dropped. Besides allowing the users to disable dropping, we propose a *smart dropping strategy* in § 4.3 to dynamically vary the accuracy, given a tolerable latency and a peak active camera set size.

For timely processing of the video feeds, it is sufficient for the latency between a frame generated at a camera and its processed response reaching the UV to fall within  $\gamma$ . This can be exploited to enhance the processing throughput by *batching events* passed to the VA/CR modules to amortize the static overheads of invoking the external DL models, while ensuring that the processing latency per event is within permissible limits. However, the time budget available for batching can vary across time, and is non-trivial to estimate without a shared global clock. Besides allowing users to set a fixed batch size, we propose an *adaptive batching strategy* in § 4.4 that maximizes the batch size without violating the latency constraint, for a given accuracy requirement and a peak active camera set size.

Data drops and dynamic batching are featured in stream processing systems. Techniques for load shedding (drops) [5, 6] and batching [21, 40] have been proposed to help determine the the fraction of data to be dropped and the batch size. They use greedy empirical approaches or model it as an optimization problem that is solved using numerical solvers. But they make centralized decisions,

are computationally costly and/or expect synchronized device clocks. These are challenging on constrained and wide-area distributed resources. Instead, we design strategies that are lightweight, distributed and resilient to clock-skews.

## 4.2 Preliminaries

For modeling latency, we decompose the dataflow graph of module instances (tasks) shown in Fig. 2 to a set of sequential task *pipelines*, with a *task selectivity* of 1:1 – the ratio of input to output events. Each sequential pipeline comprises of F, VA, CR and VU instances, though we assume these are generic tasks,  $[\tau_1, \tau_2, \dots, \tau_n]$ , where  $\tau_1$  is the source task and  $\tau_n$  is the sink task. We propose strategies for an individual pipeline, which is then generalized to the entire dataflow.

Each event  $e_k$  arriving at the source task  $\tau_1$  of each pipeline is assigned a unique ID  $k$ . This ID propagates to all its causal downstream events. Since we have a 1:1 selectivity, an event  $e_k^i$  in the pipeline can be uniquely identified by a combination of its source event ID  $k$  and the task  $\tau_i$  it is an input to.

When an event  $e_k^i$  arrives at a task  $\tau_i$  from an upstream task  $\tau_{i-1}$ , it is placed in a FIFO queue (Fig. 4). Events at the front of the queue are identified by the Executor to form a batch, whose size is dynamically decided, as discussed in § 4.4. The user-logic is triggered on the batch of input events and it returns a batch of output events that is passed to a *partitioner*, which routes each event based on its key to a downstream task. Let  $a_k^i$  indicate the *arrival time* of an event  $e_k^i$  at a task  $\tau_i$  from its upstream task (Fig. 4). This timestamp is measured at the resource hosting the task  $\tau_i$ . The time spent by the event in the queue before execution is given by the *queuing duration*  $q_k^i$ . Once events from the queue are formed into a batch of size, say  $b$ , let the function  $\xi_i(b)$  give the *estimated execution duration* for the batch by the user-logic for the task  $\tau_i$ . We assume that the *execution duration* monotonically increases with the batch size, i.e.,  $\xi(b) < \xi(b + 1)$ . When  $b = 1$ , this is a streaming execution with no batching delay. We also define the *processing duration*  $\pi_k^i = q_k^i + \xi(b)$ , as the time between an event arriving at a task and the resulting output event being placed on its output stream.

We define the *upstream time* for an event  $e_k^i$  arriving at task  $\tau_i$  as  $u_k^i = a_k^i - a_k^1$ . This is a relative time defined using the timestamps of the source event  $e_k^1$  at the source task and the causal event  $e_k^i$  observed at the current task, which in turn depend on their local device clocks  $\kappa_1$  and  $\kappa_i$ . The arrival time  $a_k^1$  for the source event  $e_k^1$  is propagated to all its causal downstream events in their headers.

While we initially assume all device clocks are synchronized, we later discuss how our techniques are resilient to clock-skews between all devices (as is common in MAN/WAN), except those hosting the source and sink tasks of the pipeline,  $\kappa_1$  and  $\kappa_n$  [17, 27].

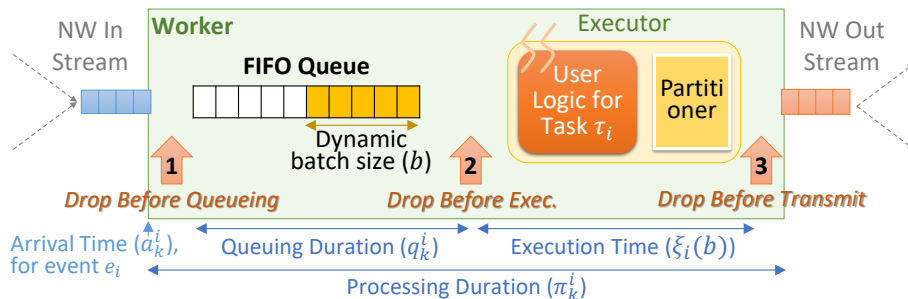


Figure 4: Processing events at a task, with batching and drops

### 4.3 Strategies to Drop Events

The platform should drop any event  $e_x^y$  that cannot reach the last task  $\tau_n$  before a time  $a_x^1 + \gamma$  as it exceeds its maximum tolerable latency  $\gamma$  and is hence *stale*. So a task  $\tau_i$  may drop an arriving event  $e_x^i$  if  $a_x^i > a_x^1 + \gamma$ . While simple, this waits till the allowed latency is exceeded and does not prevent resource wastage due to execution of tasks prior to the one where the event is dropped. E.g., if at tasks  $\tau_{n-2}$  and  $\tau_{n-1}$ , we have  $a_x^{n-2} < a_x^1 + \gamma$  and  $a_x^{n-1} > a_x^1 + \gamma$ , then every event will be processed through the first  $(n-2)$  tasks and yet dropped at the  $(n-1)^{th}$  task, assuming that the task processing times and network performance stay constant. Ideally, the first task  $\tau_1$  should reject a newly arriving event if it *will* be rejected downstream to avoid resource wastage.

We capture the potential staleness of an event at a task  $\tau_j$  using a *completion budget*  $\beta_j$ . This is the duration allowed for an arriving event to complete processing at this task, including the upstream time spent since its source task, i.e., if  $u_k^i + \pi_k^i > \beta_i$  for an event  $e_k^i$ , it is stale and can be dropped. Since  $\pi_k^i$  is not known when the event arrives but only after it is queued and executed, this drop decision is taken thrice within a task, as shown in Fig. 4 and described below.

This completion budget for a task can change often during the lifetime of an application as the system reacts to variability. Later, in § 4.5, we discuss how  $\beta_i$  is actively updated to encapsulate this variability. It guarantees that for a given budget, if the downstream tasks do not exhibit further variability, then any event that meets the budget will be processed within  $\gamma$ , and vice versa.

#### 4.3.1 Drop Point 1

The first drop decision is when an event arrives at a task but before it is placed in its input queue (Fig. 4). This checks if the observed upstream time already expended plus the fastest possible execution duration for the event on this task, i.e., using a batch size of  $b = 1$ , will cause the event to exceed its completion budget, even in the absence of any queuing. Since we do not know the actual queuing delay and batch size for this event at this time, we are conservative in this decision. So events that pass this test may still be dropped at subsequent

drop points based on how long they spent in the queue and the actual execution duration.

---

```

1: procedure DROPBEFOREQUEUING( $a_k^1, a_k^i$ )
2:    $u_k^i = a_k^i - a_k^1$ 
3:   if ( $u_k^i + \xi_i(1) \leq \beta_i$ ) then return false      ▶ Retain
4:   else return true      ▶ Drop this event
5:   end if
6: end procedure

```

---

### 4.3.2 Drop Point 2

The second drop point is after the event is queued and put in a batch, but before the batch is executed. At this time, we have a batch of events  $B$  of size  $b$ , which gives us the expected execution time  $\xi_i(b)$ , and the queuing duration  $q_k^i$  for each of its events. If the predicted time to complete executing this event exceeds the completion budget, i.e.,  $u_k^i + q_k^i + \xi_i(b) > \beta_i$ , we drop this event. The function is passed the entire batch and it returns an updated batch  $B'$  without events that should be dropped.

---

```

1: procedure DROPBEFOREEXEC( $B[ ], b$ )
2:   for  $\langle a_k^1, a_k^i, q_k^i, e_k^i \rangle$  in  $B$  do
3:      $u_k^i = a_k^i - a_k^1$ 
4:     if ( $u_k^i + q_k^i + \xi_i(b) \leq \beta_i$ ) then  $B' \leftarrow e_k^i$       ▶ Retain
5:     end if
6:   end for
7:   return  $B'$       ▶ Events that should be executed
8: end procedure

```

---

### 4.3.3 Drop Point 3

It is possible that the actual execution time was longer than estimated. So we trigger the third drop point after the batch execution, where the processing time  $\pi_k^i$  has been spent on an event, but before its output events are sent on the output stream. Here, we check if the generated event  $e_k^{i+1}$  at time  $u_k^i + \pi_k^i$  has exceeded its completion budget  $\beta_i$ . This drop point is also important if the dataflow has branches, as discussed next.

---

```

1: procedure DROPBEFORETRANSMIT( $a_k^1, a_k^i, \pi_k^i$ )
2:    $u_k^i = a_k^i - a_k^1$ 
3:   if ( $u_k^i + \pi_k^i \leq \beta_i$ ) then return false      ▶ Retain
4:   else return true      ▶ Drop this event
5:   end if
6: end procedure

```

---

By providing these three light-weight drop points, we achieve fine-grained control in avoiding wasted network or compute resources, and yet perform event drops just-in-time when they are guaranteed to exceed the budget. This balances application accuracy and performance. As a further optimization, we allow the user-logic to flag an event as *avoid drop*, e.g., if it has a positive match, and the platform avoids dropping such events even if they exceed the tolerable latency.

This can improve the accuracy and manage the active set size.

#### 4.3.4 Non-linear Pipelines

While the drop logic has been defined for a linear pipeline, a module instance (task) in our dataflow can send an event to one of several downstream module instances, based on the partitioning function. However, the destination task for an output event is known only after the partitioner operates on that event, at drop point 3. The completion budget for a task depends on the network and compute performance of the downstream tasks that the event flows through, which can vary for the different task-paths taken. So for each task, we maintain one budget per downstream task.

### 4.4 Strategies for Dynamic Batching of Events

Batching and executing events in a stream improves the throughput and reduces the average event latency [18]. When events arrive early at a task  $\tau_i$  and/or the application has a relaxed  $\gamma$ , there may adequate completion budget  $\beta_i$  to accumulate events from the input queue into a batch and execute them together, while not violating the budget and causing a drop. Since  $\beta_i$  and the input event rates can vary over time, this batch size has to be dynamically decided.

We define the *event deadline*  $\delta_k^i = \beta_i + a_k^1$  for an event  $e_k^i$  as the time at the task  $\tau_i$  by which it must complete processing to avoid being dropped. Similarly, we define the *batch deadline*  $\Delta_p^i = \min(\delta_1^i, \dots, \delta_m^i)$  as the latest time by which the batch  $B_p$  having  $m$  events must complete execution, and it is defined as the earliest event deadline among all events in the batch. Since temporal event ordering is not assumed, this may not be the first event in the batch.

The batching logic considers the event  $e_x^i$  at the head of the queue at the present time  $t_i$  for adding to the “current batch”  $B_p$  having size  $m$  by checking if  $t_i + \xi_i(m+1) > \min(\Delta_p^i, \delta_x^i)$ , i.e., will adding this event to the batch cause the new execution time of the batch ( $t_i + \xi_i(m+1)$ ) to exceed the deadline of the batch  $\Delta_p^i$  or the new event  $\delta_x^i$ . If not, we add the event to the current batch and update the batch deadline. We incrementally check and add events from the queue into the current batch. If the event at the head of the queue cannot be added to the batch, we submit the current batch for execution and add the head event to a new empty batch that becomes the current batch. Even if the queue is empty, the current batch is automatically submitted for execution when the local clock reaches the time,  $\Delta_p^i - \xi_i(m)$ .

### 4.5 Updating the Completion Budget

The *completion budget*  $\beta$  for a task is central to determining the events to be dropped as well as the batch size. To deal with the dynamism in the system, the budget for all tasks must change over time. To enable this, each task  $\tau_i$  stores a 3-tuple  $\langle d_k^i, q_k^i, m_k^i \rangle$  for every event  $e_k^i$  it has processed: the *departure time*  $d_k^i = u_k^i + \pi_k^i$ , which sums the upstream time and the processing duration; the

queuing duration  $q_k^i$ ; and the batch size  $m_k^i$  that the event was part of. Further, each downstream event sent by task  $\tau_i$  in the pipeline is augmented with two header fields: the *sum of execution times*  $\bar{\xi}_k^i = \sum_{j=1..i} \xi_j(m_k^j)$  and the *sum of the queuing delay*  $\bar{q}_k^i = \sum_{j=1..i} q_k^j$ , spent at the preceding tasks.

As an event executes through the pipeline, we either increase or decrease the budgets for the upstream tasks based on whether the event arrives at the destination task early or is dropped by a task in-between, respectively. The logic used for these budget changes are described next.

#### 4.5.1 Reducing the budget

If an event is processed within its completion budget at a task, it should also complete processing that pipeline within the maximum tolerable latency, if there is no downstream variability. However, if an event  $e_k$  gets dropped at task  $\tau_j$ , it means that the downstream latency has deteriorated and hence, the completion budget of all the upstream tasks  $\{\tau_i | i = 1..j - 1\}$  must be reduced. If the event has exceeded the completion budget by  $\epsilon = d_k^i - \beta_i$ , then the sum of the upstream completion budgets must be reduced by  $\epsilon$ . Intuitively, we reduce the budget at each upstream task  $\tau_i$  proportional to the time spent in the queue and batch before execution. This causes batches with fewer events to be formed for execution. Using just the queuing time ratio for reducing the budget also avoids penalizing tasks with longer execution times.

Let  $\overleftarrow{\lambda}_k^i$  be the duration by which the budget  $\beta_i$  at an upstream task  $\tau_i$  has to be *reduced* due to an event  $e_k^j$ , being dropped at  $\tau_j$ , where  $i < j$ .

$$\overleftarrow{\lambda}_k^i = \min\left(\epsilon \times \frac{q_k^i}{\bar{q}_k^i}, \xi_i(m_k^i) - \xi_i(1)\right)$$

The first term in the min operator reflects the excess time  $\epsilon$  scaled by the ratio of the queuing delay for the task relative to the sum of the delays at all the tasks upstream of the dropping task. The second term ensures that the budget reduction does not fall below the minimum possible budget required when streaming the event through with  $b = 1$ .

Whenever an event is dropped at  $\tau_i$ , it sends a *reject signal* to its upstream tasks with the event ID  $k$ , the excess duration over the budget  $\epsilon$  and the sum of the queuing delays  $\bar{q}_k^j$ . The receiving task  $\tau_i$  combines these with the 3-tuple it maintains for the event to calculate  $\overleftarrow{\lambda}_k^i$ , and updates its budget as:

$$\beta_i^{new} = \min(d_k^i - \overleftarrow{\lambda}_k^i, \beta_i^{old})$$

The first term determines the updated budget as the earlier departure time for that event, less the reduction in budget. Here, the min operator selects the lower of the previous and the new budget to make the model be resilient to out of order accept or reject signals.

### 4.5.2 Increasing the Budget

Events that arrive at the final task much earlier than the maximum tolerable latency indicate lost opportunity costs in improving the throughput and scalability of the pipeline by forming larger batches. Therefore, when an event arrives at the final task at  $\epsilon = \beta_n - u_k^i$  duration earlier than its completion budget  $\beta_n = \gamma$ , and this value is greater than some set threshold,  $\epsilon^{max}$ , the completion budget of the upstream tasks must be increased. Intuitively, we increase the budget of a task proportional to its execution time, relative to the total execution times for all upstream tasks. This gives more weight to tasks with longer execution times, allowing them to increase their throughput which is likely to be the least in the pipeline.

If  $\vec{\lambda}_k^i$  is the duration by which the budget  $\beta_i$  at an upstream task  $\tau_i$  has to be reduced due to an event  $e_k^n$  completing ahead of time at the final task  $\tau_n$ , then:

$$\vec{\lambda}_k^i = \min\left(\epsilon \times \frac{\xi_i(m_k^i)}{\xi_k^{n-1}}, (m^{max} - m_k^i) \times \frac{q_k^i}{m_k^i} + \xi_i(m^{max}) - \xi_i(m_k^i)\right)$$

The first term in the min operator scales the  $\epsilon$  by the relative time spent in the execution duration for the task  $\tau_i$ , relative to the execution time at all tasks until (but not including) the final task. The second term ensures that the budget does not exceed the time taken to create and execute the largest batch size  $m^{max}$  allowed by the user. This assumes that the queuing time scales linearly with the number of events. As the prior budget already considers the queuing and execution time for a batch size  $m_k^i$ , we subtract it from  $m^{max}$ .

A batch will have events with different queuing duration but the same batch execution duration. So some events in the batch will always arrive at the final task before  $\gamma$  elapses. However, we should not increase the budget based on these early events in a batch. Rather, the decision to increase the budget is made only if event with the highest latency in a batch is below  $\gamma + \epsilon^{max}$ . If so, the task  $\tau_n$  sends an *accept signal* to all the upstream tasks with the slowest event's ID  $k$ , the duration of early arrival  $\epsilon$  and the sum of upstream execution time,  $\vec{\xi}_k^{n-1}$ . These are used to calculate the value of  $\vec{\lambda}_k^i$  at tasks  $\tau_i$  and update their budgets using the 3-tuples for that event: The completion budget for an task  $\tau_j$  is increases as follows:

$$\beta_i = \max(d_k^i + \vec{\lambda}_k^i, \beta_i^{old})$$

As before, selecting the max is against the previous budget is to make the model resilient to out of order signals.

The task budgets are increased when an event successfully reaches the final task ahead of time. But transient conditions may cause the system to reduce the budgets to such a low value that no subsequent events flow through to the final task without being dropped. In such cases, even if the conditions improve, the budget may never get updated. To address this, the system periodically sends *probe signals* for every  $k^{th}$  event that is dropped at a task  $\tau_j$ . This probe is forwarded downstream without being dropped. If this signal reaches the final task within  $\gamma$ , then the system calculates and sends the *accept signal* so that the

budget for the upstream tasks can be increased and regular events may start flowing through.

When *bootstrapping* the application initially, the batch size for all tasks is fixed at  $b = 1$  and no budgets are assigned except  $\beta_n = \gamma + a_k^1$ . Subsequently, when accept or reject signals are triggered, these values are updated (without considering  $\beta^{old}$ ) and they stabilize to the new budget.

## 4.6 Formal Bounds and Time Synchronization

While our batching is not based on a fixed batch size but rather adapts to the events that arrive, we can formally bound the batch size and drop rate under certain assumptions. Later, we relax some of these assumptions.

### 4.6.1 Fixed conditions

We first derive bounds on the batch size and drop rate working under the assumption that a dataflow has constant known input rate  $\omega$ , 1:1 selectivity, no pipelining, the execution time matches the expectation, and the network and compute conditions are static. For simplicity during analysis, we also assume temporal ordering of events and no pipelining of the FIFO queue with the execution.

**Batch Size.** Here, the goal is to estimate the bounds for the *batch size*  $m_i$  at a task  $\tau_i$  when it has access to the budget and other variables at runtime, under a stable state. The inter-arrival rate between successive events can be written as  $a_k^i - a_{k+1}^i = \frac{1}{\omega} \quad \forall k \in \mathbb{N}, i \in n$ . Also, due to the temporal ordering of events, the batch deadline is bound by its first event. Then,  $m_i$  is the largest Integer value such that:

$$(m_i - 1) \times \frac{1}{\omega} + \xi_i(m) \leq \beta_i - u_1^i \quad \text{and} \quad \xi_i(m_i) \leq \frac{\beta_i - u_1^i}{2}$$

In the first equation, we capture the intuition that the time to queue up the batch and to execute it <sup>1</sup> must not exceed the batch processing deadline. The second equation ensures the stability of the system such that the time to execute a batch does not exceed the deadline for the next batch being accumulated, i.e., execution time for the current batch should be less than the queuing time for next batch. Here,  $\omega$  and  $\xi_i(m)$  are unconstrained natural numbers while  $\beta_i$  and  $u_i$  are available at runtime. A solution for  $m_i$  may not exist within these constraints, which means that the input rate  $\omega$  is unsustainable. In such cases, events should be dropped.

**Drop Rate.** If no solution for  $m_i$  exists above, then we find the *drop rate* of events,  $(\omega - \omega^{max})$ , relative to the largest stable input rate,  $\omega^{max}$ , that can be support, and the associated batch size. The goal is to maximize  $m_i$  and  $\omega^{max}$  such that:

$$(m_i - 1) \times \frac{1}{\omega^{max}} + \xi_i(m_i) \leq \beta_i - u_1^i \quad \text{and}$$

---

<sup>1</sup>There is no queuing delay for the first event, hence  $(m - 1) \times \frac{1}{\omega}$ . For simplicity, we assume that the estimated execution time  $\xi_i$  equals the actual execution time.

$$\xi_i(m_i) \leq \frac{\beta_i - u_1^i}{2}$$

Compared to streaming execution with  $m = 1$ , batching adds latency to the overall event processing time while increasing the throughput. We quantify the increase in the *average latency* per event caused by batching, relative to streaming, for a task  $\tau_i$  as:

$$\frac{m_i - 1}{2 \times \omega} + \xi_i(m_i) - \xi_i(1)$$

Here, the first term is the average queuing time for the  $m_i$  events in the batch and the latter indicate the execution time for the batch.

#### 4.6.2 Resilience to Unsynchronized Clocks

Devices in a WAN may have unmanaged devices that do not have tightly-synchronized clocks [17]. While our drop and batch decisions are based on the timestamps at the different devices, these have been designed to withstand skews across the device clocks. The drop logic as well as the completion budget are based on the *upstream time*, with the other time variables within a task being defined relative to it. So making the upstream time resilient to unsynchronized clocks with consequently address all other time calculations.

Let  $\kappa_1.. \kappa_n$  be the clocks for the  $n$  devices hosting the tasks in a pipeline. As stated before, we require that  $\kappa_1 = \kappa_n$ . Let the signed-values  $\sigma_2.. \sigma_{n-1}$  be the skew between the clocks  $\kappa_2.. \kappa_{n-1}$  relative to  $\kappa_1$  and  $\kappa_n$ , i.e.,  $\sigma_i = \kappa_i - \kappa_1$ . The upstream time  $u_k^i = a_k^i - a_k^1$  for an event  $e_k^i$  arriving at a task  $\tau_i$ . When corrected for the skew, we have  $\tilde{u}_k^i = (a_k^i - \sigma_i) - a_k^1$

Similarly the update rule for the *completion budget*  $\tilde{\beta}_i$  for task  $\tau_i$ , when corrected for skew, can be written by correcting the *departure time* as  $(\tilde{d}_k^i - \tilde{\lambda}_k^i)$  or  $(\tilde{d}_k^i + \tilde{\lambda}_k^i)$ , as is the case when updating using a reject or an accept signal. Here,  $\tilde{d}_k^i = \tilde{u}_k^i + \pi_k^i = u_k^i - \sigma_i + \pi_k^i$ , since  $\pi$  is a duration calculated locally within a single device. Also,  $\tilde{\lambda}$ , the budget change factor, depends on  $\epsilon$  and other local durations, with  $\tilde{\epsilon} = \tilde{d}_k^i - \tilde{\beta}_i = \epsilon$ . Hence  $\tilde{\beta}_i = \beta_i - \sigma_i$ , and it can be shown that  $\tilde{\beta}_i^{old} = \beta_i^{old} - \sigma_i$  with an inductive argument.

As a result, in all three of our drop points, when replacing  $u_k^i$  and  $\beta_i$  with their skew-correct forms (in lines 3, 4 and 3, respectively), we have a  $-\sigma_i$  term added symmetrically to both the left and the right sides of the comparisons, which cancel each other out. This shows that our drop logic is resilient to clock-skews.

For batching, we use the test  $(t_i + \xi_i(m+1) > \min(\Delta_p^i, \delta_x^i))$  to decide if we should add an event  $e_x^i$  arriving at task  $\tau_i$  to a batch  $B_p$ . Here too we can correct the skew for the time points  $\tilde{t}_i = t_i - \sigma_i$  and  $\tilde{\delta}_x^i = (\tilde{\beta}_i + a_k^1) = (\beta_i - \sigma_i + a_k^1) = (\delta_x^i - \sigma_i)$ ; similarly,  $\tilde{\Delta}_p^i = \Delta_p^i - \sigma_i$  as it derives from  $\tilde{\delta}$ . As we see, the  $-\sigma_i$  term is added to both the sides of the comparison and cancel each other out, indicating that the batch size is resilient to unsynchronized clocks as well.

## 5 Experiments

We perform targeted and detailed experiments to evaluate the benefits of the domain-sensitive *Tuning Triangle knobs* (Fig. 2, inset) we offer: (1) a smarter tracking logic, (2) dynamic batching capability, and (3) multi-stage dropping strategies. We empirically demonstrate our proposition that these knobs help achieve *two of the three qualitative metrics*: (1) end-to-end latency within the user-defined threshold  $\gamma$ , (2) scaling to a large number of the active cameras, and (3) the accuracy of the tracking.

### 5.1 Setup

**System Setup.** We mimic the resource conditions of 96 Raspberry Pi 3B edge devices on a local cluster, which has 1 *head node* and 10 *compute nodes*. The compute nodes each have an 8-core/16-hyperthreads @2.10 GHz Intel Xeon CPU E5-2620 v4 CPU and 64GB DDR4 RAM, while the head node has the same CPU in a dual socket configuration and 512GB RAM. Each Xeon CPU core perform comparable to a 4-core Pi 3B, as measured using the CoreMark benchmark. All the nodes have a 1Gbps network interface. The nodes run Centos v7.5 with Linux 3.10.0 kernel release, Java 1.8 and Python v3. The head node hosts a Kafka v2.11.0 pub-sub broker for routing input video streams while the compute nodes have Pytorch v1.0.1 and Tensorflow 1.2 installed.

**Anveshak Setup.** We have two Anveshak worker processes on each compute node and the head node. The number of FC instances equals the number of cameras used in that experiment. In addition, we have 10 VA, 10 CR, 1 TL and 1 UV instances. The FC instances are scheduled across the 10 compute nodes in a round-robin manner for load balancing, and run on one of the two workers on the node. The VA and CR instances are also placed in a round-robin manner on these nodes, on the other worker. This co-locates a subset of the FC, VA and CR on the same server and minimizes their network transfer overheads. Since each instance runs on a separate executor thread within the worker, each in-effect runs on a Pi 3B-class CPU core. The TL and UV instances run on a worker each on the head node.

**Applications.** We implement two tracking applications, *App 1* and *App2*, described in Table. 1 and evaluate them in our experiments. These omit the QF module given its nascency. Further, we use three TL algorithms for the applications. *TL-Base* is a naïve baseline that keeps all the cameras in the network active all the time. *TL-BFS* has access to the underlying road network, but assumes a fixed road-length for all edges when performing the spotlight BFS strategy. *TL-WBFS* is similar, but aware of the exact lengths of each road segment (Alg. 1). Both *TL-BFS* and *TL-WBFS* are configured with the *expected peak speed* of the entity being tracked, which varies across experiments. The maximum tolerable latency is set as  $\gamma = 15$  secs. We provide a detailed analysis for App 1, and confirm similar for App 2 as well.

**Workload.** For the road network, we extracted a circular region of 7  $km^2$  from *Open Street Maps* [45], centered at the Indian Institute of Science, Ban-

galore campus. This has 1,000 vertices and 2,817 edges, with an average road length of 84.5 *m*. We use this as the fixed road length for TL-BFS. We use the *CUHK03* Person Re-identification image dataset [36] with 1,360 unique targets and 10,531 images, which provide *true positives or negatives* for the models used. Each JPG image is  $64 \times 128px$  in size with RGB colors, and a median size of 2.9 *kB*.

We use these images to simulate video feeds that mimic the movement of the query entity through a road network. The simulator takes as input the road network with the road lengths, the speed of the entity being tracked, their starting vertex in the network, and the labelled images for the entity. A given number of cameras are “placed” on vertices surrounding the starting vertex. The number of cameras is 1000 by default, but varies for some experiments. We simulate the movement of the entity from the source vertex as a *random walk* at a speed of 1 *m/sec* (3.6 *km/hr*). Each camera generates a timestamped feed of images at 1 *fps* using the true negative images (i.e., images not containing the entity), but uses the true positive images for the time intervals when the tracked entity is within the camera’s FOV during the walk. For each camera, the simulator publishes its image feed in real-time to a unique topic using the Kafka broker. The FC module for the camera subscribes this appropriate topic to acquire the input stream.

**Baseline.** We also design a *near-optimal baseline (NOB)* to evaluate the effectiveness of our dynamic batching. This uses prior benchmarking on the stable system to determine the smallest batch size that can meet specific input rates without any drops or delays, for rates of 1–1000 *events/sec*, in steps of 10. This forms a lookup table. During the application execution, the platform dynamically picks the batch size for the rate closest to the current input rate from this table. Such a runtime strategy can maximize the throughput while also minimizing the latency. In fact, under static system conditions, this will be near-optimal, limited only by the discrete rates for which the table is constructed.

## 5.2 Analysis of App 1

### 5.2.1 Analysis of Batching Strategy

We first examine the benefits of the *dynamic batching* knob of the tuning triangle, while keeping the tracking logic fixed at *TL-BFS* and *disabling drops*. Further, the entity’s *peak speed* is configured as  $es = 4$  *m/sec* with TL-BFS. This is set based on an estimated peak speed since underestimating can cause the entity to be lost due to a slow *Rate of Expansion (RoE)* of the spotlight when the entity is in a blindspot; too high a value can cause a fast spotlight RoE and large active camera count that overwhelm the resources (or cause drops).

**Need for Batching.** The Anveshak dataflow can be executed in a streaming manner without batching, i.e., a batch size of  $b = 1$ . But this sacrifices the input throughput, and hence scalability of the number of active cameras that can be supported.

Fig. 7a shows the application timeline plot for the streaming configuration,

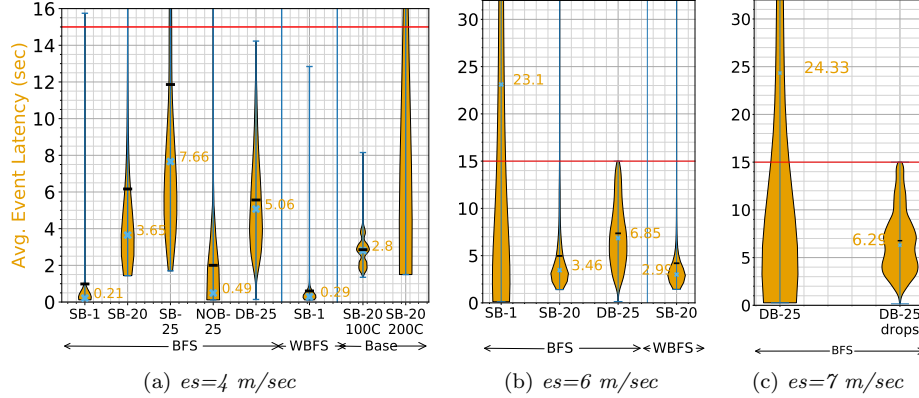


Figure 5: Distribution of the average end-to-end event latencies for the different batching and TL strategies of App 1

using a static batch of size  $b = 1$  (SB-1). Here, the X axis is the wall-clock time (secs) of the tracking application’s execution, the blue line on the left Y axis is the number of active cameras as decided by TL, and the yellow dots on the right Y axis are the end-to-end latency of events (frames) from the source to the sink averaged over every second of the application’s execution time. A red horizontal line shows the maximum tolerable latency,  $\gamma = 15 \text{ secs}$ . Further, Fig. 5a shows a violin distribution of these 1 sec average event latencies for the streaming and other batching configurations. Similarly, Fig. 6a shows the number of events ( $1000\times$ ) processed within the deadline of  $\gamma$  against those that were delayed (orange, labelled).

In Fig. 5a, streaming (SB-1) exhibits the lowest median latency, at  $\approx 200\text{ms}$ , much below  $\gamma = 15 \text{ secs}$  that is acceptable. However, this is at the cost of the latency occasionally exceeding the threshold, as seen from the violin outliers, and the 25 delayed events in Fig. 6a. In fact, if we configure TL with an entity peak speed of  $es = 6 \text{ m/s}$ , 57% of the input events exceed  $\gamma$  when streaming (Fig. 6b).

As Fig. 7a shows, these delayed frames occur when the active camera count exceeds 100. Here, the blue lines exhibit a saw-tooth behavior – the spotlight logic increases the active set of cameras when the entity is in a blindspot, and this drops to 1 when the entity is reacquired within the FOV of an active camera. At  $\approx 550 \text{ secs}$ , the entity is in a blindspot long enough that the count spikes to 111 cameras, stressing the available resources and causing the latency to grow to 16.8 secs.

Specifically, this latency is caused by CR, whose DNN is the slowest task the dataflow at  $120 \text{ ms/event}$  and can service  $\mu = \frac{1000}{120} = 8.33 \text{ events/sec}$  per CR instance. For an event arrival rate  $\lambda > \mu$ , the queue is unstable and the queuing delays will grow exponentially. At the  $550^{\text{th}}$  second, the feeds from 111 active cameras at 1 fps are mapped to 10 CR instances, and 8 of these CR instances

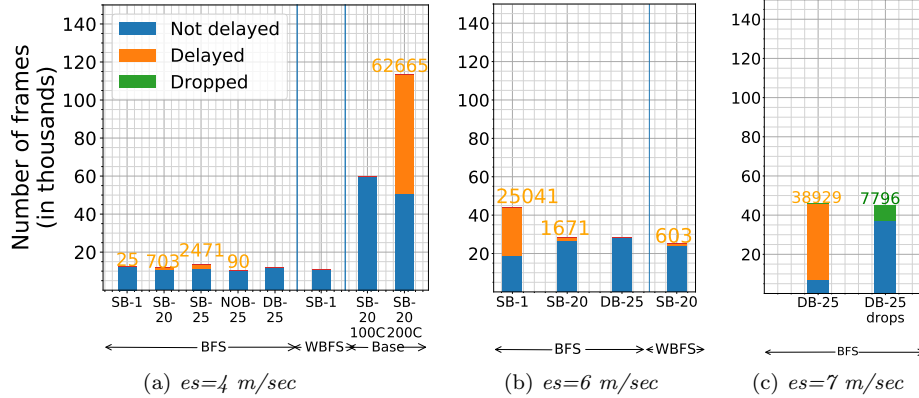


Figure 6: Events with latency  $\leq \gamma$  vs. Delayed vs. Dropped events, for different peak speeds, batching and TL strategies

receive events faster than  $\mu$  causing a spike in the event latency. However, in this case, the system is able to recover at  $\approx 570$  secs when the active set size drops to 1.

In summary, it is vital to process *all* the frames in a *timely* manner rather than *many* in a *fast* manner, i.e., taking up to but below  $\gamma$  is better. Batching offers such efficiencies and helps scale to a larger number of active cameras.

**Limitations of Static Batching.** While batching improves the system throughput, using a fixed or static batch size has two limitations. There can be a missed detection of the entity or certain frames can experience a very high end-to-end latency. Next, we provide empirical evidence for this.

We first set the static batch size  $b = 20$  for all tasks, and report its latency, active camera count and events processed without delay in Figs. 7b, 5a and 6a, as before. We see that the median latency has increased to 3.65 secs in Fig. 5a, and there are no sharp growths in the latency in Fig. 7b which would indicate an unstable queue. Interestingly, in periods where the active camera count increases, like between 140–240 secs, the mean latency decreases – more cameras means a higher input rate, which fills up a batch and triggers it faster, thus reducing batching delays.

But better stability does not always result in fewer latency violations. In Fig. 6a, we see 6% or 703 events exceed  $\gamma$ , more than the streaming case. Since the batch size is fixed, *there is no bound* on the time spent by an event waiting for the batch to be completed before execution. This causes events to be delayed. However, if using  $es = 6$  m/s, none of the input events exceed  $\gamma$  (Fig. 6b). This too indicates that a fixed value of the batch size will not suffice for all situations. Selecting an appropriate peak latency  $\gamma$  and peak speed  $es$  by the domain user is also important.

Another consequence of event delays due to a large fixed batch size is that TL grows the spotlight larger than necessary as it receives negative detections

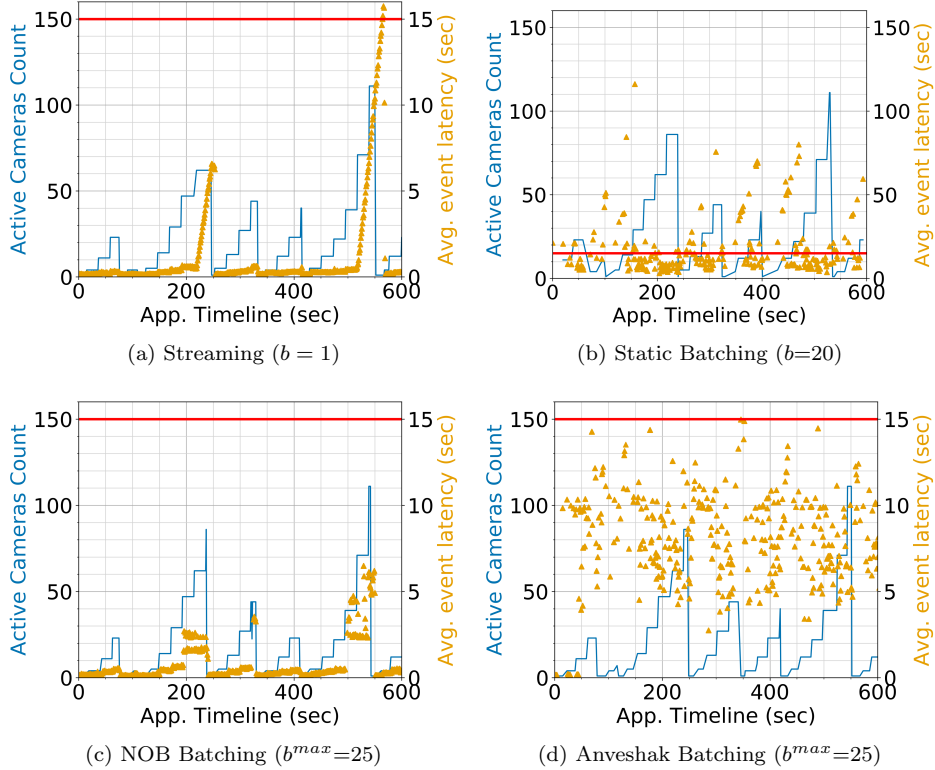


Figure 7: # of active cameras (left Y axis, blue line) and Avg. end-to-end event latency (right Y axis, yellow dots) over Application execution timeline (X axis) for different batching strategies, TL-BFS,  $es = 4$  m/sec. Red horizontal line shows  $\gamma = 15$  secs.

of the entity late, and also delays shrinking the spotlight as positive detections arrive late. These put further stress on the resources. E.g., at the 220<sup>th</sup> second, the active set size is 62, 86 and 139 using a batch sizes of  $b = 1, 20$  and 25 (latter is not plotted), due to the increase in median latency from 0.2 sec to 3.65 secs and 7.6 sec (Fig. 5a). When  $b = 25$ , there is a delay of 22 secs in detecting a missing entity, due to which the active camera count sharply jumps to 139, and also causes a detection of the entity in the neighboring cameras to be missed. In fact, 22% of events are delayed for  $b = 25$  (Fig. 6a).

**Benefits of Dynamic Batching.** The varying number of active cameras and its consequence on the latency is a strong motivation for using a dynamic batch size. Here, we compare Anveshak’s dynamic batching strategy with the Near-optimal Baseline (NOB) dynamic batching strategy. The maximum batch size is limited to  $b^{max} = 25$  for both.

The timeline plot for NOB and our dynamic batching (DB-25) are shown

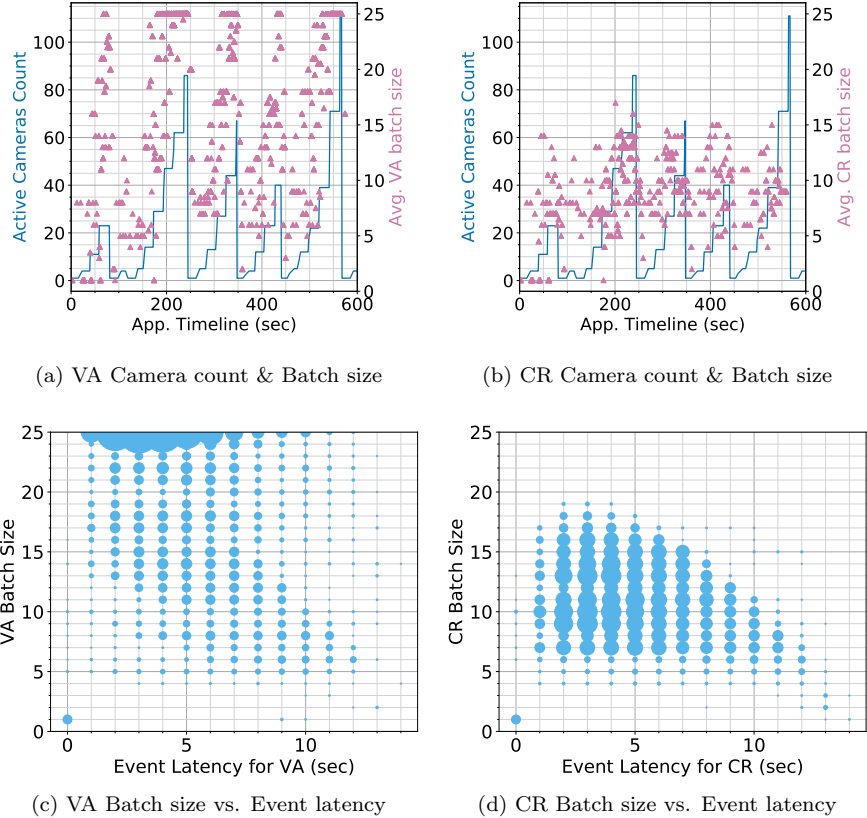


Figure 8: Performance of Anveshak batching, TL-BFS,  $es=4$  m/s

in Figs. 7c and 7d, with their latency distribution and delay frames listed in Figs. 5a and 6a. The key observation is that there are no delayed events in Anveshak’s batching while 90 events are delayed for NOB, at time periods 350 secs and 520 secs. The latter is despite selecting a near-optimal batch size from the lookup table as the system is executing. Even minor runtime variations cause a larger batch size to be selected, leading to events being queued longer when forming the batch and delaying them. But Anveshak’s batching prevents delays in *all cases*.

NOB does offer a lower latency distribution, at a median of 0.4 secs (Fig. 5a). The batch size it chooses is often between 2 and 5, thus approaching a streaming scenario. The median latency for Anveshak’s batching is 7.66 secs, with a wide variety of batch sizes. But as discussed before, reducing the latency is not a goal; just ensuring that all events reach within  $\gamma$ .

**Analysis of Anveshak’s Batching.** We further analyze the behavior of Anveshak’s dynamic batching by examining the two key tasks that dominate

the execution latency, VA and CR. The dynamic batch sizing operates independently for these two tasks types.

Figs. 8a and 8b show the active cameras count (left Y axis) and the batch size averaged every 1 sec (right Y axis), for all 10 VA and CR tasks for the application execution time-time (X Axis), while Figs. 8c and 8d show a bubble (scatter) plot of the task latency per event against the batch size the event was part of, for all VA and CR instances.

For the *VA task*, we see from Fig. 8a that the batch size increases as the active camera count grows, helping it support a higher input event throughput. VA uses almost every batch size between 1 and 25 (Fig. 8c), and the latency varies within a single batch size – events in a batch that arrive later will have a lower latency, and vice versa. For the larger batch sizes, the task latency often ranges from 2–6 secs, indicating that the VA module can benefit from a more relaxed  $b^{max}$ .

The *CR task* shows a similar trend between the camera count and batch size in Fig. 8b. CR has a lower mean batch size than VA, which is expected since the CR module is a compute intensive DNN which has a larger execution time than the VA module. Fig. 8b which is a timeline plot for mean number of CR shows a similar trend. Also, despite  $b^{max} = 25$ , its peak batch size never exceeds 19.

On further analysis, the maximum budget allocated to a CR task is  $\beta = 3.65$  secs. At the peak active camera count of 111, this task receives events from 13 cameras. For forming a batch of size  $b = 25$ , we have its queuing time as 1.92 secs, assuming a uniform input rate of 13 events/sec, and execution time of  $\xi(25) = 1.74$  secs, which together at 3.66 secs exceed the budget. Instead, the dynamic batch size selected of  $b = 19$  results in a processing time of 2.91 secs, which is within the budget. This indicates that Anveshak’s dynamic batch sizing is sensitive to the needs of individual tasks well. In fact, even with a peak entity speed of  $es = 6$  m/sec, it is able to avoid any event delays (Fig. 6b, DB-25).

**Adapting to network variation.** The complexity of Anveshak’s batching logic is partly attributed to its ability to respond to handling network and computation variability. The former is more common in WAN and MAN. We evaluate its ability to adapt to even sharp changes in the network performance. Using the dynamic setup for Anveshak and NOB from Figs. 7c and 7d, we drop the bandwidth between compute nodes from 1 Gbps to 30 Mbps midway through the application execution at 300 secs into the timeline. These are shown in Figs. 9a and 9b for Anveshak and NOB.

The first 300 secs is identical to the earlier plots, and neither configuration has event delays. But once the bandwidth drops, Anveshak manages to keep the system stable with no event delay as it reacts to event latencies increasing. As the network degrades, the budget available to tasks reduce, causing smaller batch sizes to be formed. The median CR batch size rapidly drops from  $b = 8$  to 5, and the batches with 1 and 2 events rise from only  $\approx 18\%$  before 300 secs to  $\approx 30\%$  after the network slowdown. However, NOB becomes unstable and its event latency grows beyond  $\gamma$  after 500 secs. This is due to its lookup table being created for a certain system performance and that not holding at runtime.

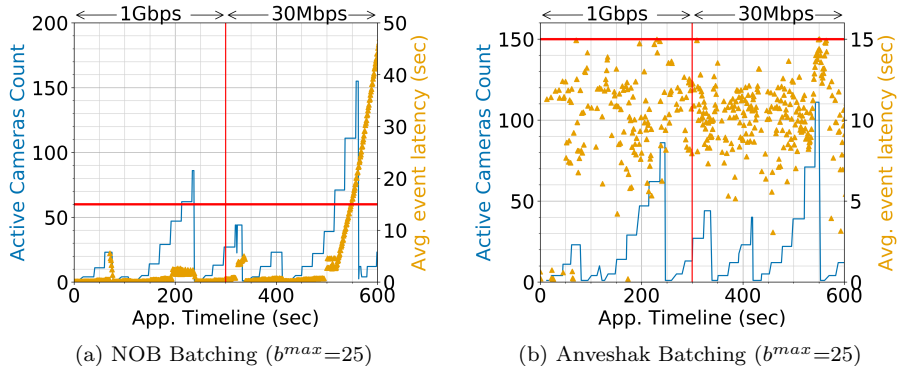


Figure 9: Adapting to network variation. The system bandwidth drops from 1 Gbps to 30 Mbps after the 300<sup>th</sup> sec.

### 5.2.2 Analysis of Tracking Logic

We next consider the benefits of the tracking logic knob of the tuning triangle in helping control the active camera count and scalability of Anveshak. We compare the prior *TL-BFS* logic with two others, *TL-Base* that is simpler, and *TL-WBFS* that is more advanced. We use static batching, keep drops disabled and  $es = 4$  m/sec.

*TL-Base* is a baseline logic that keeps all cameras active, similar to contemporary systems. Since the resources are inadequate to support all 1000 cameras being active, we do two runs, with 100 and 200 cameras placed on a proportionally smaller road network, and all active. We use a static batch size of  $b = 20$ , which offers the best configuration. Fig. 10b plots the application time-line and the event latency averaged over 1 sec for the 100 and 200 camera setup. While the event latency is stable without any delays for 100 cameras, it is unstable and grows rapidly with 200 active cameras, indicating a lack of resources. The total frames processed is  $\approx 60,000$  in the former, and  $\approx 120,000$  in the latter with over 55% delayed (Fig. 6a, Base SB-20 100c and 200c). Obviously, this does not scale to 1000 cameras, unlike our runs with better TL algorithms.

The more advanced TL strategy *TL-WBFS* supports 1000 total cameras on the same set of resources by being smarter about which ones are activated. It supports a stable latency with  $b = 1$  streaming (Fig. 10a) with no events delayed (Fig. 6a, WBFS SB-1), in contrast to *TL-BFS* which was unstable for  $b = 1$  (Fig. 7a). The active camera count grows in more granular steps using *WBFS* since it is aware of the road lengths and leads to a more measured growth of active cameras. Further, its peak active camera count is 67, relative to 111 when using *TL-BFS*. So *WBFS* can help scale to a larger set of total cameras or for a longer period of the entity being in a blindspot.

While a better TL helps, it is not a substitute for dynamic batching since we can have scenarios where a static batch is not adequate. E.g., for a faster

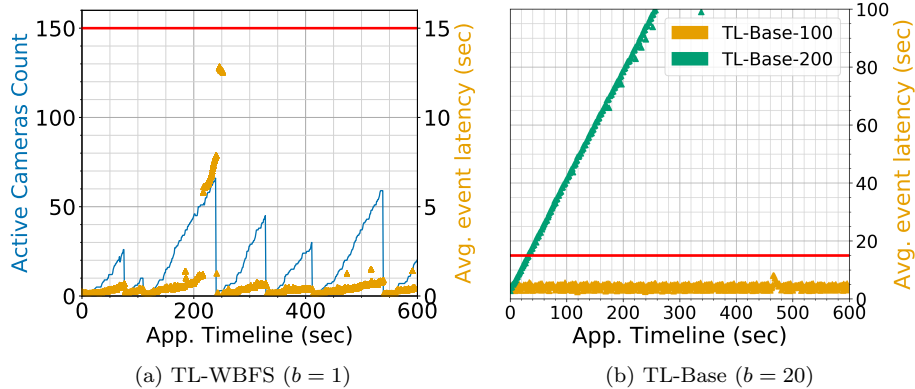


Figure 10: Effect of *tracking logic* on performance,  $es=4$  *m/sec*

$es = 6$  *m/sec*, TL-BFS with a static batch size of  $b = 20$  causes 603 events to be delayed, compared to no delays when using dynamic batching (Fig. 6b, BFS SB-20 vs. DB-25).

### 5.2.3 Analysis of Dropping Strategy

Even TL and dynamic batching may not suffice when the spotlight grows large. This can cause the resources to be overwhelmed, latencies to grow unabated, and cascade to all future events. Anveshak’s smart dropping strategy is beneficial here to drop events early in the pipeline to avoid resource wastage, and reduce overall event delays.

We run the App 1 experiments from § 5.2.1, using our dynamic batching and TL-BFS, but with a faster peak walk speed of  $es = 7$  *m/s*. This causes the spotlight to grow faster when the entity is in a blindspot. Under such conditions, when *drops are disabled*, we see from the timeline plot in Fig. 11a that the application is unstable, with latency  $\gg \gamma$  as the active cameras grow from 100–500. This causes each CR instance to receive a peak of  $\approx 49$  *events/sec*, while its capacity is only 19 *events/sec*. This results in 85% of events to be delayed (Fig. 6c, DB-25).

When *drops are enabled*, the application’s latency is stable and within  $\gamma = 15$  *secs* even when the active camera count grows as high as 389 (Fig. 11b). The drops start when the camera count exceeds 200, which matches  $\approx 20$  *events/sec* for each CR task. While 17% of all events are dropped, the rest of the events are processed without any delays (Fig. 6c, DB-25 Drops). Dropping frames containing the entity can delay locating the entity and cause the active set to grow. However, none of the 21 frames carrying the detected entity is dropped. This is merely incidental, but enabling the *do not drop* flag will actually ensure this. The batch sizes for VA and CR are smaller here (not shown) than for  $es = 4$  *m/sec* with dynamic batching but no drops (Figs. 8c and 8d). When the

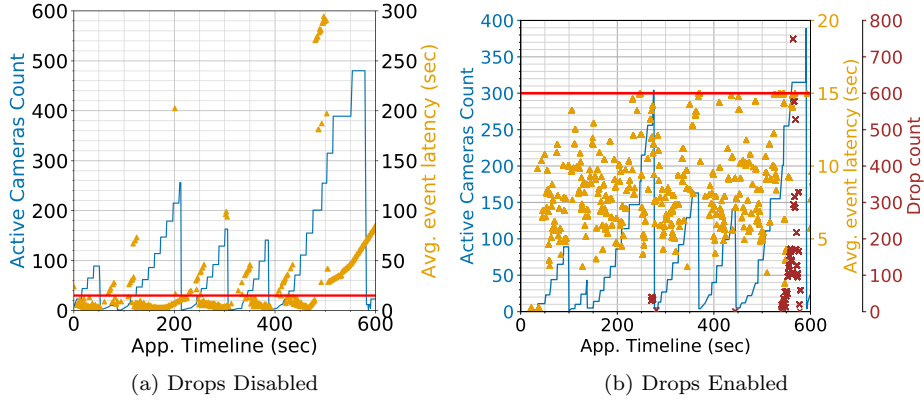


Figure 11: Perf. with *drops dis/enabled*, *TL-BFS* and  $es=7$  *m/sec*

input event rate is high, the system first reduces the queuing time by forming smaller batches and then resorts to drops.

### 5.3 Analysis of App 2

In this section, we perform a subset of the above experiments for App 2 to reconfirm the tuning triangle trends. The key difference between these two applications is CR, with the logic for App 2 using a more accurate and compute-intensive DNN that takes  $\approx 63\%$  longer to process each frame than for App 1. We use the same road network, entity query, 1000-camera setup,  $\gamma = 15$  *secs*, BFS tracking logic, drops disabled and peak entity speed of  $es = 4$  *m/s* by default, unless mentioned otherwise. Figs. 12 show the *latency distribution* and the *number of delayed events* for App 2, for various runs, while Fig. 12c shows the *active camera count* for App 1 and App 2 using BFS and WBFS TL along the application timeline.

Using a static batch size of  $b = 20$ , we observe a median latency of 4.33 *secs* but with  $\approx 5\%$  latency violation (Figs. 12a and 12b, BFS SB-20). But with dynamic batching enabled with  $b^{max} = 25$ , we see a median latency of 5.39 *secs* but crucially, no latency delays for events (Figs. 12a and 12b, BFS DB-25). This confirms the need for and benefits of *dynamic batching* in App 2 as well.

The tracking logic in App 2 plays an important role in managing the growth in the active camera set size, similar to App 1. In Fig. 12c, using a static batch size of  $b = 20$ , we see that TL-WBFS, which uses the knowledge of road lengths for its spotlight expansion, has a more modest increase in camera count, e.g., at  $\approx 500$  *secs*, compared to TL-BFS. This help it scale to a denser camera deployment or a longer duration of the entity being in a blindspot. Both App 1 and App 2 have similar camera count patterns, partly modulated by the different CRs used.

Finally, for  $es = 6$  *m/s* we see that dynamic batching is inadequate for TL-

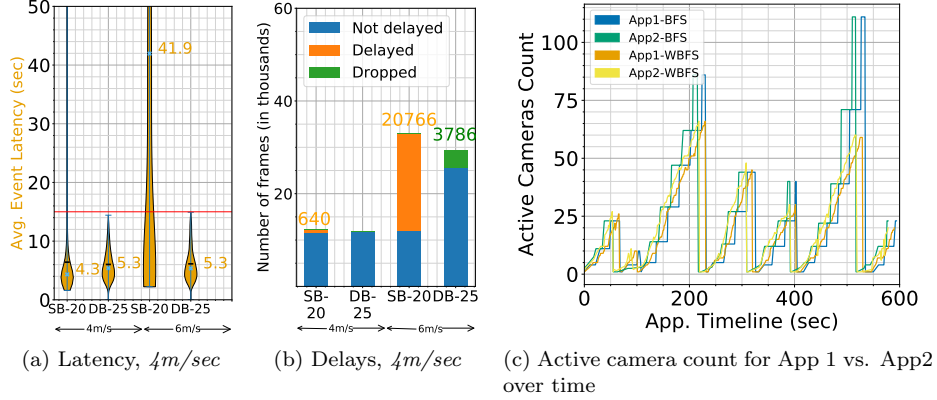


Figure 12: Latency distribution, event delays and camera count for different configurations of *App 2*, using *TL-BFS*

BFS as it reports a median latency of 41.95 *secs* and 63% of events delayed (Figs. 12a and 12b, BFS DB-25). But by enabling drops, this reduces the drops to  $\approx 12\%$  with other events being processed within time, with a median latency of 5.36 *secs* (BFS DB-25 Drops). Here again, App 2 exhibits the value of *proactive and intelligent drops* by Anveshak rather than allow delayed events to flow through and waste resources.

## 6 Related Work

**Video Surveillance Systems.** Intelligent video surveillance systems allow automated analytics over camera feeds [11]. They enable wide-area surveillance from multiple static or PTZ cameras, with distributed or master-slave controls [44]. *ADVISOR* [52] supports tracking, crowd counting, and behavioral analysis over camera feeds from train stations to support human operators. However, these are pre-defined applications, run centrally on a private data center and process all camera feeds all the time. *IBM's Smart Surveillance System (S3)* [51] is a proprietary platform for video data management, analysis and real-time alerts. While it offers limited composability using different modules, it too executes the applications centrally and does not consider performance optimizations. Early works examine edge computing for basic pre-processing [34]. But the edge logic is statically defined, with the rest of the analytics done centrally and over dedicated networks.

The *Ella middleware* [23] supports the definition of distributed analytics on the edge and over a WAN. They use a publish-subscribe model with hierarchical brokers to route video and event streams between analytics deployed on edge devices. They illustrate a multi-camera single person tracking application, similar to us. However, their platform design resembles a general-purpose

event-driven middleware, without any specific model support or runtime optimizations for video analytics, unlike us. Others exclusively focus on offline analysis over video feeds from a many-camera network along with other data sources for spatio-temporal association studies [49].

*Vigil* [59] is designed for video surveillance on wireless networks with limited bandwidth. They assume an Edge computing node (ECN) is co-located with the cameras and is used to reduce redundant data from being sent to the Cloud. The authors assign a utility score to each frame to ascertain its importance, similar to our *do not drop* flag. Our model and platform offer more active controls over the logic running on the ECN, and the runtime tuning.

*EdgeEye* [38] efficiently deploys DNN models on the edge using a JavaScript API for users to specify their parameters. While it caters to a wider class of analytics applications, it lacks composability and domain-specific patterns for tracking applications. It offers performance optimizing for the DNN model, but does not consider distributed systems issues, such as batching, dropping and network variability. *Video Storm* [58] is a video analytics system with the goals of approximation and delay tolerance. It schedules video analytics query workloads on a cluster of machines, where each query has a deadline and priority. *Video Edge* [29] extends this to support scheduling on a hierarchy of edge, fog and cloud resources. Both these provide tuning knobs which are conceptually similar to our ours. But the key distinction is that these degrees of freedom requires the specification of objective functions to define the impact of the knobs on metrics. This makes it challenging to use out of the box. Our domain-sensitive Tuning Triangle more intuitively captures the impact of the three well-defined knobs on the three metrics that have the most impact on tracking applications.

While we propose and demonstrate several graph-based tracking logic, probability-based and spatio-temporal models have been explored in literature. Jain, et al. [30] perform an empirical evaluation of spatio-temporal constraints and correlations, and leverage these to improve the precision and reduce computational cost of cross-camera video analytics. Others [50] perform offline analysis to learn the spatio-temporal constraints between cameras. During the online tracking phase, these are used to prune the number of potential paths. Kalman Filter has also been used to estimate the motion probability of the object being tracked [31].

**Big Data platforms and DSL.** Generic stream processing platforms like *Apache Storm*, *Flink* and *Spark Streaming* [19, 55, 57] offer flexible dataflow composition. But defining a domain-specific dataflow pattern for tracking applications, like we do, offers users a frame of reference for designing distributed video analytics applications, with modular user-defined tasks.

*Google's TensorFlow* [7] is a DSL for defining DNNs and CV algorithms, and to deploy trained models for inference. However, TensorFlow is not meant for composing arbitrary modules together. The tasks take a Tensor as an input and give a Tensor as the output, and there are no native patterns such as Map and Reduce to ease composability. Yahoo's *TensorFlow on Spark* [3] gives more flexibility by allowing Spark's Executors to feed RDD data into TensorFlow.

Thus, users can couple Spark’s operations with TensorFlow’s neural networks. But Anveshak is at a level of abstraction higher, allowing for rapid development of tracking applications with fewer lines of code or sometimes just a configuration change. Also, Spark is not designed for distributed computing on WANs or edge/fog devices, which we address in the Anveshak runtime.

**Streaming Performance Management.** There are several performance optimization approaches adopted by stream processing systems, which we extend. *Apache Flink* [19] and *Storm* [55] support *back-pressure*, where a slow task sends signals to its upstream task to reduce its input rate. This may eventually lead to data drops, but the data being dropped are the new ones generated upstream rather than the stale ones that are already in-flight, which sacrifices freshness in favor of fairness. Our drops prioritize recent events over stale events, and also adjust the budget more precisely.

*Google’s Millwheel* [10] uses the concept of *low watermarks* to determine the progress of the system, defined as the timestamp of the oldest unprocessed event in the system. It guarantees that no event older than the watermark may enter the system. Watermarks can thus be used to trigger computations such as window operations safely. While our batching and drop strategies are similar, watermarks cannot budget the time left for a message in the pipeline and has no notion of user-defined latency.

*Aurora* [6] use the concept of *load shedding*, which is similar to our data drops. They define QoS as a multidimensional function, including attributes such as response time, similar to our maximum latency. Given this function, the objective is to maximize the QoS. *Borealis* [5] extends this to a distributed setup. Anveshak uses multiple drop points even within a task, which offers fine-grained control and robustness. Features like “do not drop” and resilience to clock skews are other domain and system-specific optimizations.

## 7 Conclusions

In this paper, we have proposed an intuitive domain-specific dataflow model for composing distributed object tracking applications over a many-camera network. Besides offering an expressive and concise pattern, we surface the Tracking Logic module as a powerful abstraction that can perform intelligent tracking and manage the active cameras. This enhances the scalability of the application and makes efficient use of resources. Further, we offer tunable runtime strategies for dropping and batching that help users easily balance between the goals of performance, accuracy and scalability. Our design is sensitive to the unique needs of a many-camera tracking domain and for distributed edge, fog and cloud resources on wide-area networks. Our experiments validate these for a real-tracking application on feeds from up to 1000 cameras.

As future work, we plan to explore intelligent scheduling of the module instances on edge, fog and cloud resources; allow modules to be dynamically replaced for better accuracy or performance; handle mobile camera platforms such as drones. In a real setting, multiple objects of interest would be tracked

across the camera network. This should lead to interesting scheduling problems as well as an opportunity to share compute across multiple queries.

## 8 Acknowledgments

We thank Prof. A. Chakraborty, Visual Computing Lab, IISc, for discussions on the tracking problem and video analytics modules. We also thank fellow students, Swapnil Gandhi and Anubhav Guleria, for their valuable insights. This work was supported by grants from Huawei as part of the Innovation Lab for Intelligent Data Analytics and Cloud, and resources provided by Microsoft and NVIDIA.

## References

- [1] How many CCTV cameras are there in London? <https://www.cctv.co.uk/how-many-cctv-cameras-are-there-in-london/>. Accessed: 2018/07/28.
- [2] Open-ReID. <https://cysu.github.io/open-reid/>.
- [3] Tensorflow on Spark. <https://github.com/yahoo/TensorFlowOnSpark/wiki>. Accessed: 2018/06/16.
- [4] . Kubernetes. <http://kubernetes.io/>, 2020.
- [5] Daniel J Abadi, Yanif Ahmad, Magdalena Balazinska, Ugur Cetintemel, Mitch Cherniack, Jeong-Hyon Hwang, Wolfgang Lindner, Anurag Maskey, Alex Rasin, Esther Ryzkina, et al. The design of the borealis stream processing engine. In *Cidr*, volume 5, pages 277–289, 2005.
- [6] Daniel J Abadi, Don Carney, Ugur Çetintemel, Mitch Cherniack, Christian Convey, Sangdon Lee, Michael Stonebraker, Nesime Tatbul, and Stan Zdonik. Aurora: a new model and architecture for data stream management. *the VLDB Journal*, 12(2):120–139, 2003.
- [7] Martin Abadi, Paul Barham, Jianmin Chen, Zhifeng Chen, Andy Davis, Jeffrey Dean, Matthieu Devin, Sanjay Ghemawat, Geoffrey Irving, Michael Isard, Manjunath Kudlur, Josh Levenberg, Rajat Monga, Sherry Moore, Derek G. Murray, Benoit Steiner, Paul Tucker, Vijay Vasudevan, Pete Warden, Martin Wicke, Yuan Yu, and Xiaoqiang Zheng. Tensorflow: A system for large-scale machine learning. In *OSDI 16*, pages 265–283, 2016.
- [8] Ejaz Ahmed, Michael Jones, and Tim K Marks. An improved deep learning architecture for person re-identification. In *CVPR*, pages 3908–3916, 2015.
- [9] Faruk Akgul. *ZeroMQ*. Packt Publishing, 2013.

- [10] Tyler Akidau, Alex Balikov, Kaya Bekiroğlu, Slava Chernyak, Josh Haberman, Reuven Lax, Sam McVeety, Daniel Mills, Paul Nordstrom, and Sam Whittle. Millwheel: fault-tolerant stream processing at internet scale. *Proceedings of the VLDB Endowment*, 6(11):1033–1044, 2013.
- [11] Mayssaa Al Najjar, Milad Ghantous, and Magdy Bayoumi. *Video surveillance for sensor platforms: Algorithms and Architectures*. Springer, 2014.
- [12] G. Ananthanarayanan, P. Bahl, P. Bodk, K. Chintalapudi, M. Philipose, L. Ravindranath, and S. Sinha. Real-time video analytics: The killer app for edge computing. *Computer*, 50(10):58–67, 2017.
- [13] Roberto Arroyo, J Javier Yebes, Luis M Bergasa, Iván G Daza, and Javier Almazán. Expert video-surveillance system for real-time detection of suspicious behaviors in shopping malls. *Expert systems with Applications*, 42(21):7991–8005, 2015.
- [14] Apurva Bedagkar-Gala and Shishir K Shah. A survey of approaches and trends in person re-identification. *Image and Vision Computing*, 32(4):270–286, 2014.
- [15] Flavio Bonomi. Cloud and fog computing: trade-offs and applications. In *Intl. Symp. Comp. Architecture (ISCA)*, 2011.
- [16] Daniel P Bovet and Marco Cesati. *Understanding the Linux Kernel: from I/O ports to process management*. ” O’Reilly Media, Inc.”, 2005.
- [17] Florian Buchholz and Brett Tjaden. A brief study of time. *digital investigation*, 4:31–42, 2007.
- [18] Alfredo Canziani, Adam Paszke, and Eugenio Culurciello. An analysis of deep neural network models for practical applications. *CoRR*, abs/1605.07678, 2016.
- [19] Paris Carbone, Asterios Katsifodimos, Stephan Ewen, Volker Markl, Seif Haridi, and Kostas Tzoumas. Apache flink: Stream and batch processing in a single engine. *Bulletin of the IEEE Computer Society Technical Committee on Data Engineering*, 36(4), 2015.
- [20] Navneet Dalal and Bill Triggs. Histograms of oriented gradients for human detection. In *CVPR*, volume 1, pages 886–893. IEEE, 2005.
- [21] Tathagata Das, Yuan Zhong, Ion Stoica, and Scott Shenker. Adaptive stream processing using dynamic batch sizing. In *Proceedings of the ACM Symposium on Cloud Computing*, pages 1–13. ACM, 2014.
- [22] Jeffrey Dean and Sanjay Ghemawat. Mapreduce: simplified data processing on large clusters. *Communications of the ACM*, 51(1):107–113, 2008.

- [23] Bernhard Dieber, Jennifer Simonjan, Lukas Esterle, Bernhard Rinner, Georg Nebehay, Roman Pflugfelder, and Gustavo Javier Fernandez. Ella: Middleware for multi-camera surveillance in heterogeneous visual sensor networks. In *Distributed Smart Cameras (ICDSC), 2013 Seventh International Conference on*, pages 1–6. IEEE, 2013.
- [24] Lukas Esterle, Peter R Lewis, Martin Bogdanski, Bernhard Rinner, and Xin Yao. A socio-economic approach to online vision graph generation and handover in distributed smart camera networks. In *ICDSC*, pages 1–6. IEEE, 2011.
- [25] Lukas Esterle, Peter R. Lewis, Richie McBride, and Xin Yao. The future of camera networks: Staying smart in a chaotic world. In *Proceedings of the 11th International Conference on Distributed Smart Cameras, ICDSC 2017*, pages 163–168, 2017.
- [26] David Fleet and Yair Weiss. Optical flow estimation. In *Handbook of mathematical models in computer vision*, pages 237–257. Springer, 2006.
- [27] Yilong Geng, Shiyu Liu, Zi Yin, Ashish Naik, Balaji Prabhakar, Mendel Rosenblum, and Amin Vahdat. Exploiting a natural network effect for scalable, fine-grained clock synchronization. In *15th USENIX Symposium on Networked Systems Design and Implementation (NSDI 18)*, pages 81–94, 2018.
- [28] Kaiming He, Xiangyu Zhang, Shaoqing Ren, and Jian Sun. Deep residual learning for image recognition. In *CVPR*, pages 770–778, 2016.
- [29] Chien-Chun Hung, Ganesh Ananthanarayanan, Peter Bodik, Leana Golubchik, Minlan Yu, Paramvir Bahl, and Matthai Philipose. Videoedge: Processing camera streams using hierarchical clusters. In *2018 IEEE/ACM Symposium on Edge Computing (SEC)*, pages 115–131. IEEE, 2018.
- [30] Samvit Jain, Junchen Jiang, Yuanchao Shu, Ganesh Ananthanarayanan, and Joseph Gonzalez. Rexcam: Resource-efficient, cross-camera video analytics at enterprise scale. *arXiv preprint arXiv:1811.01268*, 2018.
- [31] Jinman Kang, Isaac Cohen, and Gerard Medioni. Persistent objects tracking across multiple non overlapping cameras. In *2005 Seventh IEEE Workshops on Applications of Computer Vision (WACV/MOTION’05)-Volume 1*, volume 2, pages 112–119. IEEE, 2005.
- [32] Aakash Khochare, Pushkara Ravindra, Siva Prakash Reddy, and Yogesh Simmhan. Distributed video analytics across edge and cloud using echo. In *International Conference on Service-Oriented Computing (ICSOC) Demo*, 2017.
- [33] Teddy Ko. A survey on behavior analysis in video surveillance for homeland security applications. 2008.

- [34] AJ Kornecki. Middleware for distributed video surveillance. *IEEE Distributed Systems Online*, 9(2), 2008.
- [35] Yann LeCun, Yoshua Bengio, and Geoffrey Hinton. Deep learning. *nature*, 521(7553):436, 2015.
- [36] Wei Li, Rui Zhao, Tong Xiao, and Xiaogang Wang. Deepreid: Deep filter pairing neural network for person re-identification. In *CVPR*, 2014.
- [37] Mei Kuan Lim, Szeling Tang, and Chee Seng Chan. isurveillance: Intelligent framework for multiple events detection in surveillance videos. *Expert Systems with Applications*, 41(10):4704–4715, 2014.
- [38] Peng Liu, Bozhao Qi, and Suman Banerjee. Edgeeye: An edge service framework for real-time intelligent video analytics. In *Proceedings of the 1st International Workshop on Edge Systems, Analytics and Networking, EdgeSys'18*, pages 1–6, New York, NY, USA, 2018. ACM.
- [39] Xinchun Liu, Wu Liu, Huadong Ma, and Huiyuan Fu. Large-scale vehicle re-identification in urban surveillance videos. In *Multimedia and Expo (ICME), 2016 IEEE International Conference on*, pages 1–6. IEEE, 2016.
- [40] Björn Lohrmann, Peter Janacik, and Odej Kao. Elastic stream processing with latency guarantees. In *2015 IEEE 35th International Conference on Distributed Computing Systems*, pages 399–410. IEEE, 2015.
- [41] Pedro Garcia Lopez, Alberto Montresor, Dick Epema, Anwitaman Datta, Teruo Higashino, Adriana Iamnitchi, Marinho Barcellos, Pascal Felber, and Etienne Riviere. Edge-centric computing: Vision and challenges. *SIGCOMM Computer Communication Reviews*, 45(5), October 2015.
- [42] Navaneet Murthy, Ravi Kiran Sarvadevabhatla, R Venkatesh Babu, and Anirban Chakraborty. Deep sequential multi-camera feature fusion for person re-identification. *arXiv preprint arXiv:1807.07295*, 2018.
- [43] Nazmus S Nafi and Jamil Y Khan. A vanet based intelligent road traffic signalling system. In *ATNAC*, pages 1–6. IEEE, 2012.
- [44] Prabhu Natarajan, Pradeep K. Atrey, and Mohan Kankanhalli. Multi-camera coordination and control in surveillance systems: A survey. *ACM Trans. Multimedia Comput. Commun. Appl.*, 11(4), June 2015.
- [45] OpenStreetMap contributors. Planet dump retrieved from <https://planet.osm.org>. <https://www.openstreetmap.org>, 2017.
- [46] Fatih Porikli, Yuri Ivanov, and Tetsuji Haga. Robust abandoned object detection using dual foregrounds. *EURASIP Journal on Advances in Signal Processing*, 2008:30, 2008.
- [47] Joseph Redmon and Ali Farhadi. Yolo9000: better, faster, stronger. *arXiv preprint*, 2017.

- [48] Mahadev Satyanarayanan, Pieter Simoens, Yu Xiao, Padmanabhan Pillai, Zhuo Chen, Kiryong Ha, Wenlu Hu, and Brandon Amos. Edge analytics in the internet of things. *IEEE Pervasive Computing*, 14(2):24–31, 2015.
- [49] Z. Shao, J. Cai, and Z. Wang. Smart monitoring cameras driven intelligent processing to big surveillance video data. *IEEE Transactions on Big Data*, 4(1):105–116, 2018.
- [50] KA Shiva Kumar, KR Ramakrishnan, and GN Rathna. Distributed person of interest tracking in camera networks. In *ICDSC*, pages 131–137. ACM, 2017.
- [51] Chiao-Fe Shu, Arun Hampapur, Max Lu, Lisa Brown, Jonathan Connell, Andrew Senior, and Yingli Tian. Ibm smart surveillance system (s3): a open and extensible framework for event based surveillance. In *Advanced Video and Signal Based Surveillance, 2005. AVSS 2005. IEEE Conference on*, pages 318–323. IEEE, 2005.
- [52] Nils T Siebel and Steve Maybank. The advisor visual surveillance system. In *ECCV 2004 workshop applications of computer vision (ACV)*, volume 1, 2004.
- [53] Jakub Sochor, Jakub Špaňhel, and Adam Herout. Boxcars: Improving fine-grained recognition of vehicles using 3-d bounding boxes in traffic surveillance. *IEEE Transactions on Intelligent Transportation Systems*, 2018.
- [54] Christian Szegedy, Sergey Ioffe, Vincent Vanhoucke, and Alexander A Alemi. Inception-v4, inception-resnet and the impact of residual connections on learning. In *AAAI*, volume 4, page 12, 2017.
- [55] Ankit Toshniwal, Siddarth Taneja, Amit Shukla, Karthik Ramasamy, Jignesh M Patel, Sanjeev Kulkarni, Jason Jackson, Krishna Gade, Maosong Fu, Jake Donham, et al. Storm@ twitter. In *Proceedings of the 2014 ACM SIGMOD international conference on Management of data*, pages 147–156. ACM, 2014.
- [56] Prateeksha Varshney and Yogesh Simmhan. Characterizing application scheduling on edge, fog, and cloud computing resources. *Software: Practice and Experience*, 2019.
- [57] Matei Zaharia, Mosharaf Chowdhury, Michael J Franklin, Scott Shenker, and Ion Stoica. Spark: Cluster computing with working sets. *HotCloud*, 10(10-10):95, 2010.
- [58] Haoyu Zhang, Ganesh Ananthanarayanan, Peter Bodik, Matthai Philipose, Paramvir Bahl, and Michael J Freedman. Live video analytics at scale with approximation and delay-tolerance. In *NSDI*, volume 9, page 1, 2017.

- [59] Tan Zhang, Aakanksha Chowdhery, Paramvir (Victor) Bahl, Kyle Jamieson, and Suman Banerjee. The design and implementation of a wireless video surveillance system. In *Proceedings of the 21st Annual International Conference on Mobile Computing and Networking, MobiCom '15*, pages 426–438, New York, NY, USA, 2015. ACM.